AD/A-004 046

INTERPRETATION OF MICROWAVE ANTENNA RESULTS FROM A REENTRY FLIGHT TEST: A COMPARISON OF METHODS

John F. Lennon, et al

Air Force Cambridge Research Laboratories
Hanscom Air Force Base, Massachusetts

19 August 1974

Unclassified

SECURITY CLASSIFICATION OF THIS PAGE (When Data Entered)

REPORT DOCUMENTATION PAGE		READ INSTRUCTIONS BEFORE COMPLETING FORM
1. REPORT NUMBER AFCRL-TR-74-0389	2. GOVT ACCESSION NO.	3. RECIPIENT'S CATALOG NUMBER AD/A-004046
4. TITLE (and Subtitle) INTERPRETATION OF MICROWAVE ANTENNA RESULTS FROM A REENTRY FLIGHT TEST: A COMPARISON OF METHODS		5. TYPE OF REPORT & PERIOD COVERED Scientific. Interim 6. PERFORMING ORG. REPORT NUMBER PSRP No. 600
7. AUTHOR(s) John F. Lennon and J. Leon Poirier		8. CONTRACT OR GRANT NUMBER(s)
9. PERFORMING ORGANIZATION NAME AND ADDRESS Air Force Cambridge Research Laboratories (LZP) Hanscom AFB Massachusetts 01731		10. PROGRAM ELEMENT, PROJECT, TASK AREA & WORK UNIT NUMBERS 61102F, 681305 21530102
11. CONTROLLING OFFICE NAME AND ADDRESS Air Force Cambridge Research Laboratories (LZP) Hanscom AFB Massachusetts 01731		12. REPORT DATE 19 August 1974 13. NUMBER OF PAGES 53
14. MONITORING AGENCY NAME & ADDRESS(if different from Controlling Office)		15. SECURITY CLASS. (of this report) Unclassified 15a. DECLASSIFICATION/DOWNGRADING SCHEDULE

16. DISTRIBUTION STATEMENT (of this Report)

Approved for public release; distribution unlimited.

17. DISTRIBUTION STATEMENT (of the abstract entered in Block 20, if different from Report)

18. SUPPLEMENTARY NOTES

TECH, OTHER

19. KEY WORDS (Continue on reverse side if necessary and identify by block number)

Microwave flight test measurements
Ionized flow field results
Reentry flight test
Electromagnetics
Antenna/Plasma interactions

20. ABSTRACT (Continue on reverse side if necessary and identify by block number)

The AFCRL Trailblazer II reentry vehicle flight tests had two aims: first, to study reentry ionization, in particular, its effect on microwave signals; and second, to examine methods for controlling the plasma to improve antenna performance. The development of theoretical models that describe both the flow properties and their effect on antennas is an important requirement for predicting the signal attenuation, pattern distortion, and breakdown effects that can occur during reentry.

PRICES SUBJECT TO CHANGE

DD FORM 1 JAN 73 1473 EDITION OF 1 NOV 65 IS OBSOLETE

Unclassified

SECURITY CLASSIFICATION OF THIS PAGE (When Data Entered)

This is one of a series of reports on the Trailblazer II program. The particular aspect treated here involves the unmodified expansion-region plasma and its effect on an antenna located on the vehicle shoulder. This report describes some of the theoretical approaches used, discusses the levels of approximation involved, and shows the agreement between these various methods and the test data.

The failure of a single set of assumptions to yield consistent agreement over a range of altitudes confirms the need to adopt flow models appropriate to the changing regimes encountered during reentry. One significant conclusion is that performance characteristics such as reflection and interantenna coupling which depend mostly on the level of peak electron density can be represented by simple plane wave, as well as by the more sophisticated slot antenna models. The latter approach, however, is necessary to describe propagation across the entire plasma sheath.

Preface

The authors acknowledge the efforts of a number of individuals who contributed to the many aspects of data interpretation and analysis included in this report. The over-all program was under the supervision of W. Rotman, Chief of the Hypersonic Electromagnetics Branch. Dr. R. Fante developed the slot antenna theory which was used extensively, and offered many helpful comments and suggestions. Dr. R. Papa provided a number of results from his complete plane wave solution, which served to enhance the comparisons. Finally, J. Antonucci was of considerable assistance in the areas of computation and data reduction.

Contents

Illustrations

Tables

Symbols and Abbreviations

A	reference area
C_D	drag coefficient
I_A	roll moment of inertia
I_T	pitch moment of inertia
P	power; ground receiving site
R	radius; power reflection coefficient
R_{12}	power reflection coefficient (uniform, semi-infinite plasma)
S	wetted length
$S\,L$	signal loss
V	velocity
W/C_DA	vehicle weight to drag ratio
a	half length: small aperture dimension
b	half length: large aperture dimension
d_E	effective plasma slab thickness
n_e	electron density
r	slant range; antenna to ground site
x, y, z	coordinate axes
α	angle of attack; attenuation constant
β	phase constant
Δ	shock layer thickness
δ_{12}	relative phase difference

Symbols

θ	polar angle
λ_p	signal wavelength in plasma
ν	collision frequency
ϕ	azimuth angle
ϕ_o	spin angle
ψ	look angle

Superscript

'	alternate coordinate system

Subscript

A	attenuation
E	initial reentry conditions
g	received at ground
Inc	incident
MAX	maximum
N	nose
R	reflection
rec	received
ref	reflected
0	free space conditions
∞	free stream conditions

Interpretation of Microwave Antenna Results from a Reentry Flight Test: A Comparison of Methods

1. INTRODUCTION AND BACKGROUND

The research in reentry physics at the Air Force Cambridge Research Laboratories includes a flight test program involving the use of Trailblazer II rockets for the study of the properties of the reentry plasma sheath. Particular emphasis has been given to the interaction of the ionized medium with microwave antennas mounted on the vehicle. Details of the various flights have been presented in a number of reports.[1-4]

Antennas were located in the stagnation region at the nose of the vehicle on the first two launches and in the expansion region at the vehicle shoulder on the remaining flights. The variation in reentry environment over the altitude range

(Received for publication 19 August 1974)

1. Poirier, J.L., Rotman, W., Hayes, D.T., and Lennon, J.F. (1969) Effects of the Reentry Plasma Sheath on Microwave Antenna Performance: Trailblazer II Rocket Results of 18 June 1967, AFCRL-69-0354.
2. Hayes, D.T. (1972) Electrostatic probe measurements of flow field characteristics of a blunt body reentry vehicle, AIAA Paper 72-694, 5th Fluid and Plasma Dynamics Conference, Boston, Mass.
3. Hayes, D.T., Herskovitz, S.B., Lennon, J.F., and Poirier, J.L. (1972) Preliminary Report on the Trailblazer II Chemical Alleviation Flight of 28 July 1972, AFCRL-72-0640.
4. Rotman, W., Maloney, L.R. (1973) High Power Microwave Antenna Performance in the Stagnation Region of a Blunt Reentry Nose Cone, AFCRL-TR-73-0072.

of the tests, together with differences in flow properties at the various antenna positions on the vehicles, has resulted in an extensive body of data on microwave signal performance in a nonuniform ionized medium. Subsidiary localized measurements of the ionization levels at various locations were obtained mainly by flush-mounted electrostatic probes,[5] although some additional diagnostic devices[6-8] were also included on the vehicles.

The flight tests have entered a second phase during which the primary objective is to modify the properties of the ionized shock layer around the vehicle by addition of chemicals to the flow. The purpose is to reduce the number of free electrons over the antenna system and hence eliminate the performance limitation imposed by the shock ionized air. Preliminary information on one of these (the fourth in the series) has been reported.[3] This additive experiment involved a shoulder antenna; the data from the third flight served to identify the plasma conditions at that location for an antenna in the absence of any alleviant.

This report is concerned primarily with the performance of microwave antennas in an unmodified plasma. The purpose is to describe some of the numerous theoretical techniques employed in the analysis of the antenna data. The use of various approximations will be discussed, the degree of agreement between different methods and test data will be shown, and the nature of some areas of disagreement will be considered.

The data which formed the basis of this analysis were obtained during the reentry portion of the Trailblazer II trajectory. A brief description of the vehicle, the experimental payload, and the flight performance will place the antenna-plasma interaction in perspective.

The reentry nose cone was launched on a Trailblazer II vehicle, a four-stage solid-propellant rocket. After the first two stages drive the vehicle to an altitude of about 200 miles, the last two stages propel the reentry nose cone back toward the atmosphere in an almost vertical trajectory.

During the ascending part of the flight, the vehicle is fin-stabilized. Shortly after launch, the canted second-stage fins induce spinning. As the vehicle leaves the atmosphere, its spin rate is high enough to ensure that it will be spin-stabilized throughout the remainder of the flight.

---

5. Hayes, D.T. and Rotman, W. (1973) Microwave and electrostatic probe measurements on a blunt reentry vehicle, AIAA Journal 11:(No. 5)675-682.
6. Lustig, C.D. and Hayes, D.T. (1969) Observation of electroacoustic resonance in a reentry sheath, Proc. IEEE 57(5):800-802.
7. Karas, N.V. (1972) Microstrip Plasma Probe, AFCRL-TR-72-0417.
8. Aisenberg, S. and Chang, K.W. (1971) Chemical Additives and Diagnostics for High Temperature Air Plasmas, AFCRL-TR-72-0354, Final Rpt, Contract No. AF19(628)-71-C-0077.

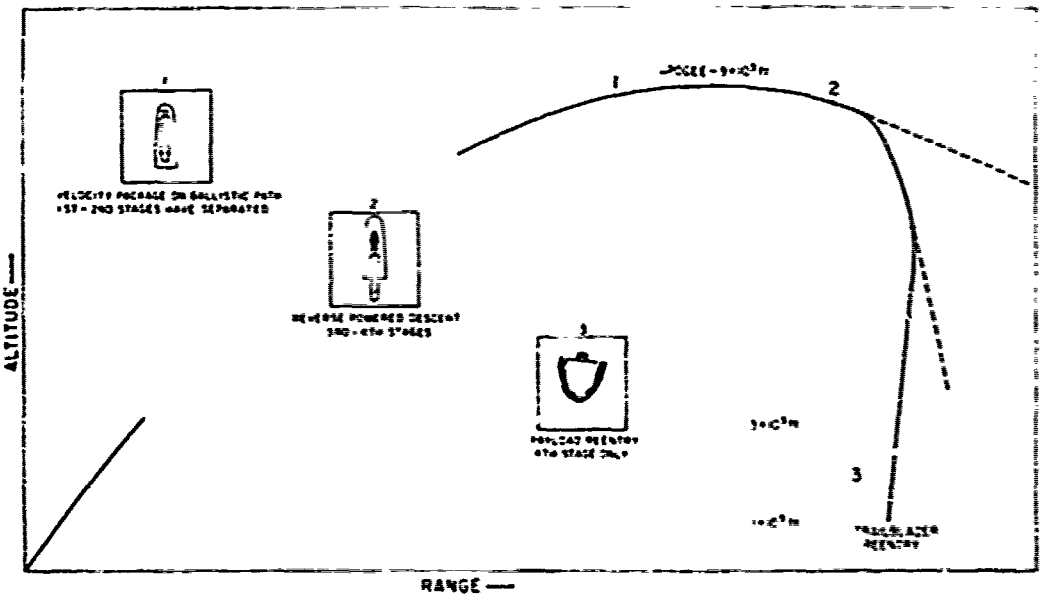

Figure 1. General Features of a Typical Trailblazer II Trajectory

The last two stages are enclosed in a structural shell (velocity package) as shown in Figure 1 and face rearward during launch. At about 250 kft, the velocity package separates from the spent second-stage motor and coasts to apogee. As the velocity package begins its descent, the X-248 third-stage motor fires, propelling the reentry nose cone out of the open end of the velocity package. The fourth-stage, 15-inch spherical motor provides the final thrust necessary to boost the nose velocity to about 17,000 fps by the time the nose cone begins reentry.

The reentry nose cone shown in Figure 2 is a 9° hemisphere-cone fabricated entirely of aluminum. Its dimensions are: nose cap radius, 6.333 in.; total length, 26.47 in.; and base diameter, 19.17 in. The instrumented nose cone weighs about 72 lb, including the spent fourth-stage motor which remains within the reentry body. The third flight was designed to obtain data in the presence of a pure-air plasma. Thus a heat-sink method of thermal protection was used to ensure that the flow around the vehicle should remain uncontaminated by ablation products.

The payload of the third flight as shown in Figure 3 is typical of the first phase flights.[9] It contains a telemetry system, a number of probe devices, and

9. Lennon, J. F. (1973) Trailblazer II Rocket Tests on the Reentry Plasma Sheath: Vehicle Performance and Plasma Predictions (Flights No. 1-3), AFCRL-TR-73-0317.

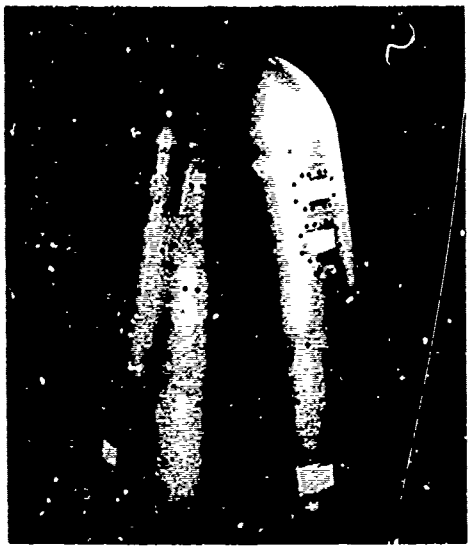

Figure 2. Reentry Stage of the Trailblazer II

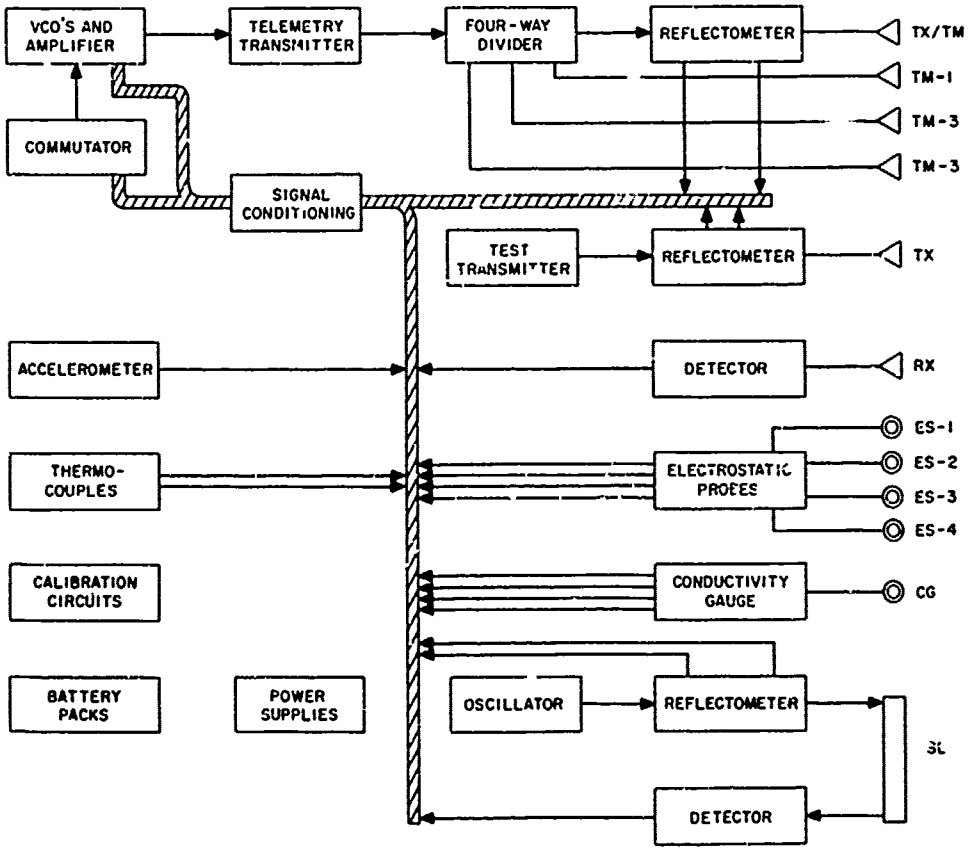

Figure 3. Block Diagram of Payload

S-band test transmitting and receiving systems. The S-band (2220.5 MHz) telemetry system antennas were mounted at the base of the cone, transmitting the flight measurements to receiving stations on the ground. The various probes were distributed along the vehicle surface, in order to obtain results under different conditions. All probes were flush-mounted instruments which measured local properties near the wall; for example, the electrostatic probes determined electron and ion densities in a sheath region adjacent to the surface, whose thickness depended on the probe bias potential. For some probes the bias level was periodically varied during the flight in order to obtain results at several distances from the surface. The electrostatic probe data have been analyzed by Hayes.[2] Good agreement between theory and observed values was obtained only near the nose region. On the side of the vehicle, there were differences both in the magnitude of the electron density and in the profile slope normal to the wall. There was some degree of consistency, however, between the probe results and the microwave data for that region. The relative positions of the probes and antennas on the third flight are shown in Figure 4 and listed in Table 1. As can be seen, electrostatic probes were placed immediately behind the test antennas so that a direct comparison could be made between microwave measurements and the local charged particle densities indicated by the probes.

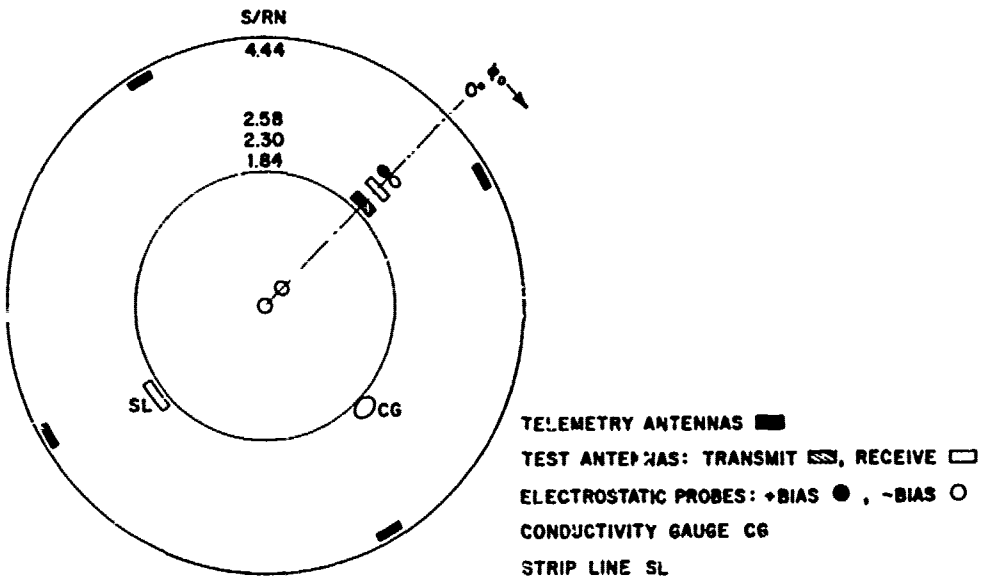

Figure 4. Relative Locations of the Antennas and Probes

Table 1. Antenna and Probe Locations and Identifications

Device	Symbol	Bias Voltage	Station (in.)	S/R_N	ϕ_o Clockwise
Electrostatic Probes	ES-1	Negative 15	0	0	-
	ES-2	Negative 5, 15, 30	0.70	0.47	0^o
	ES-3	Negative 5, 15, 30	12.62	2.58	4.5^o
	ES-4	Positive 15	12.62	2.58	355.0^o
Test Antenna Transmit	TX	-	8.03	1.84	0^o
Test Antenna Receive	RX	-	10.91	2.30	0^o
Telemetry Antennas	TM-1	-	24.27	4.44	105.5^o
	TM-2	-			195.5^o
	TM-3	-			285.5^o
Secondary Test/ Telemetry Antenna	TX/TM	-			15.5^o
Strip Line	SL	-	10.91	1.84	186.0^o
Conductivity Gauge	CG	-			90.0^o

The test antennas were located in a region where the plasma would have a significant effect on their performance, whereas the telemetry antenna location was chosen to minimize plasma interference. This is reflected in the different range of altitudes for which particular types of data are available.

Information on attenuation, for instance, which requires that the test antenna signal be received at a ground site was obtainable only until signal blackout occurred in the shoulder region. On the other hand, results for interantenna coupling and signal reflection, which are vehicle oriented measurements, continued as long as the processed data could be received from the telemetry antennas at the rear of the vehicle.

The particular plasma conditions for the experiments were determined by the flight performance of the reentry vehicle. Most of the data of interest here came from the third flight. For this reason, its flight dynamics will be cited as background for the experiment, although all flights have shown similar performance

Table 2. Comparison of Flight Parameters for the First Three Flights

Property	Flight I	Flight II	Flight III
Launch	1532 hours (EDT) 18 Jun 1967	2156 hours (EDT) 17 Jun 1969	1856 hours (EST) 24 Nov 1970
Payload weight	64.65 lb	74 lb	70.65 lb
W/C_DA	79 lb/ft^2	90.4 lb/ft^2	86.3 lb/ft^2
Spin rate	8 rps	12 rps	11 rps
I_T	1.094 slug ft^2	1.049 slug ft^2	.924 slug ft^2
I_A	0.471 slug ft^2	0.470 slug ft^2	0.510 slug ft^2
Center of gravity (Distance from nose)	10.0 in.	9.17 in.	9.76 in.
Apogee	902,183 ft	964,395 ft	990,548 ft
Peak velocity	16,593 fps (at 220 kft)	17,287 fps (at 220 kft)	17,972 fps at 216.5 kft)
Initial angle of attack	$12^o48'$	$15^o28'$	$10^o6'$
Reentry flight Azimuth	357.5^o(estimate)	286^o	31^o
Time from launch to reentry (300 kft)	392.7 sec	404 sec	405.4 sec
Third-stage burn time	29 sec	38.5 sec	40.8 sec
Fourth-stage burn time	5 sec	6 sec	9.4 sec
Initial coning: allowed value	3.45 rps	5.37 rps	5.33 rps

characteristics. This can be seen in Table 2, a comparison of various parameters for the three cases. Lennon[9] gives further details on the over-all performance of these flights.

Significant flight events are indicated on the vehicle trajectory as shown in Figure 5. The velocity and altitude histories based on time from launch can be seen in Figure 6. A peak velocity of about 18,000 fps was attained. This was the highest value recorded for any of the flights. The shock strength which depends on the velocity also would have been slightly greater for this case, resulting in somewhat higher heating and ionization levels. The trajectory data are based on radar tracking. By the time the vehicle has reached 120 kft, the air density has caused significant deceleration. The radar data on these flights become unreliable below 90 kft. Whether this can be attributed to effects relating to some surface melting of the aluminum from the aerodynamic heating, or to a break in radar tracking lock owing to the onset of high deceleration levels at these altitudes has not been resolved.

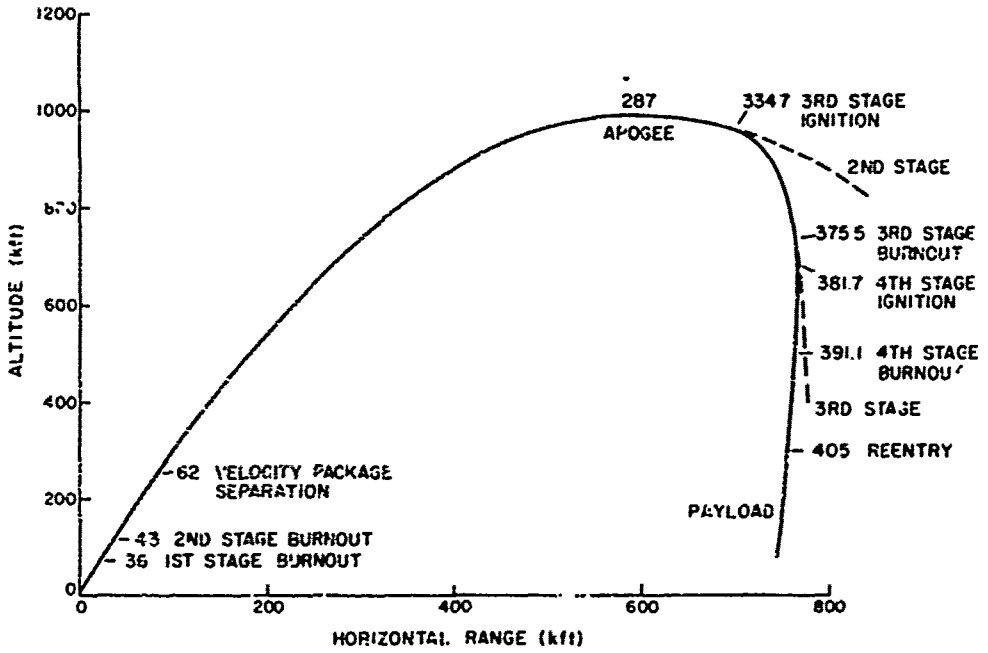

Figure 5. Trailblazer II Trajectory for the Third Flight

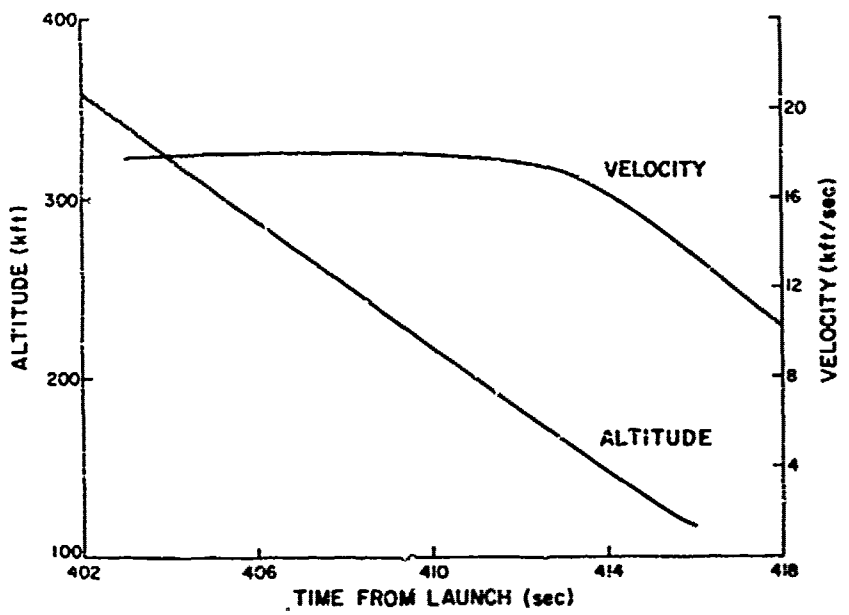

Figure 6. Trajectory Altitude and Velocity Profiles

A number of interrelated factors affected the motion of the payload. Below 500 kft, its thrust ceased and freefall began; above 200 kft, there was no significant drag acting on the vehicle. In addition, stabilization required that the vehicle be spinning. When this feature is combined with the fact that the nose cone was at an initial 10° angle of attack (as indicated by the radar data), a further complication was introduced: the ionized airflow was no longer symmetrical. The nonuniform plasma conditions were seen cyclically by the sensors as their position rotated, a fact that must be accounted for in the data analysis. Further, any changes in the original spin or vehicle orientation would be reflected in the electrostatic probe response and the microwave transmission data, that is, the effective rate of change of the local plasma conditions would assume a new value. Figure 7 shows that the frequency of cyclic variations in the data was constant for the higher altitudes. Precession does not appear until around 200 kft, where the air density has begun to be significant. The initial modulation was at a constant 10.8 Hz, and due solely to vehicle spin. The onset of atmospheric forces introduced an additional precession component. Figure 7 shows this as an increasing frequency for the cyclic response. These forces also acted to suppress the nose cone angle of attack, but this was somewhat counterbalanced by the high spin rate. A theoretical history of the vehicle orientation was calculated for the parameters

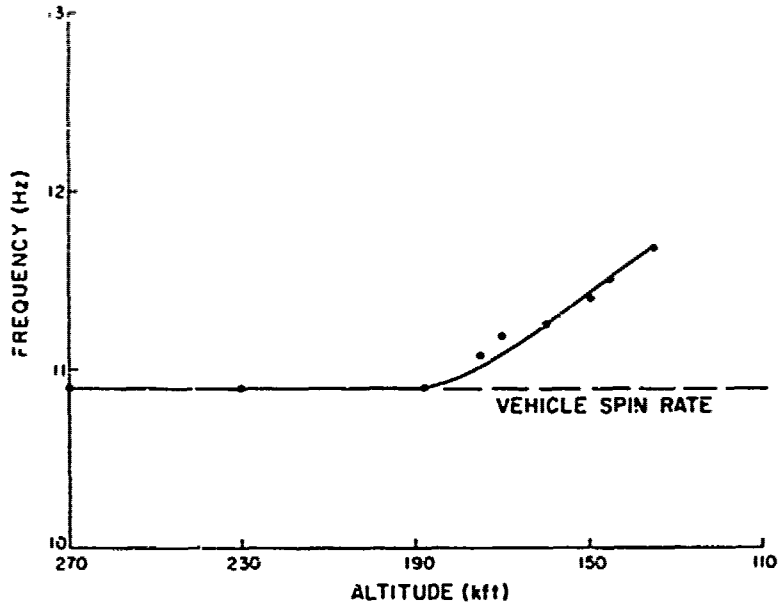

Figure 7. Frequency of Cyclic Variations in the Test Data

of the third flight. The decrease in magnitude of the angle of attack envelope is shown in Figure 8 for both spin and nonspin conditions. For practical purposes, the envelope is unchanged for the spin case, except for the final seconds.

The relative location of the reentry nose cone with respect to the ground receiving sites is shown in Figure 9 for three altitudes. The slant range between the main base and the vehicle was effectively a constant. The almost vertical reentry (8^{O} from normal) as shown by the surface projection of each of the three vehicle positions confirms that assumption. Thus, changes in received signal intensity were related only to plasma effects.

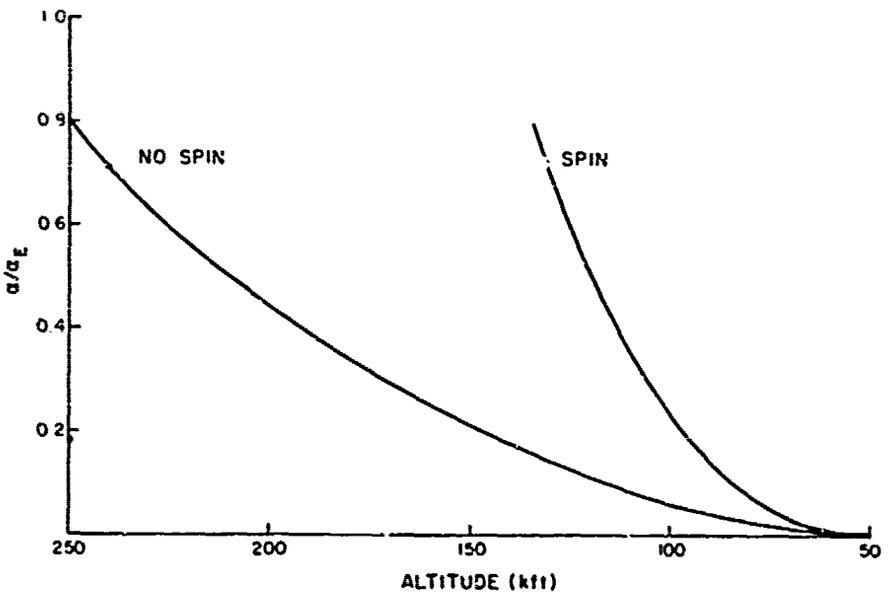

Figure 8. Computed Angle of Attack Envelope

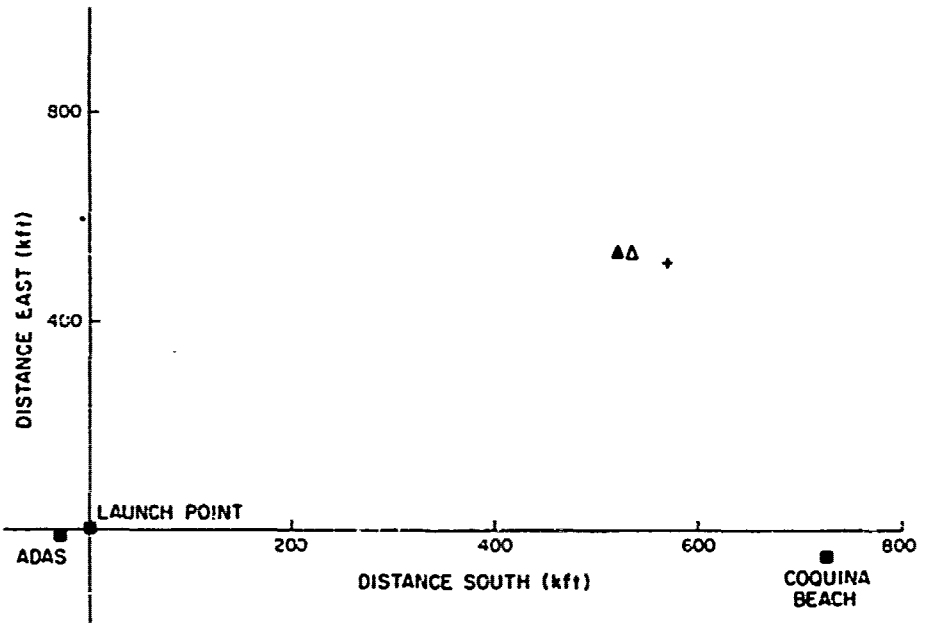

Figure 9. Geographical Orientation of Vehicle to Ground Stations During Descent: ▲ 100 kft, △ 15 kft, + 500 kft

2. S-BAND TEST SYSTEM

2.1 Description of Experiment

In this section, a brief description of the S-band test system is given, together with the manner in which the various microwave system performance parameters are determined. The specific quantities measured during reentry are antenna impedance mismatch, interantenna coupling, antenna pattern distortion, and signal attenuation.

A block diagram of the S-band experiment is shown in Figure 10. The rocket-borne portion of the system consists of a solid-state 2.5 W transmitter connected to its antenna through a reflectometer for monitoring the power reflection coefficient of the antenna. The directional coupler samples the incident power P_{inc}, and the circulator measures the reflected power P_{ref}. The transmitting antenna, as shown in Figure 11, was located a little behind the hemisphere-cone junction. Another antenna, electrically identical to the first, served as a receiving antenna; it was located further back on the vehicle and in line with the transmitting antenna. The signal power P_{rec} at this antenna is a measure of the coupling between the receiving and transmitting antennas. The transmitting antenna reflectometer output signals and the receiving antenna detector output signal are

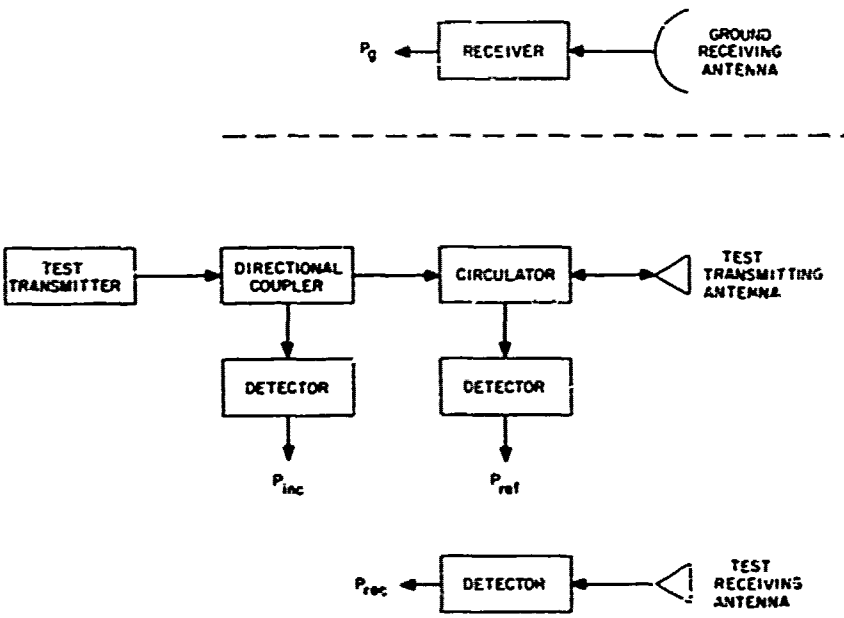

Figure 10. Block Diagram of the S-Band Test System

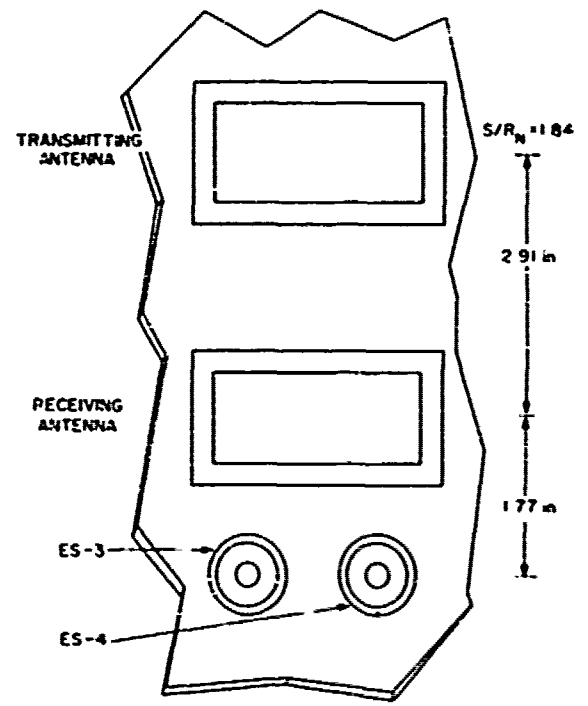

Figure 11. Cutaway View of Vehicle Surface Showing S-Band Test System

amplified to a suitable level (0-5V) and transmitted to the ground by the telemetry system.

The signal power P_g, which is received at a ground station is used in conjunction with the telemetered rocket-borne measurements to determine antenna pattern distortion of the transmitting antenna and the attenuation suffered by the transmitted signal as it propagates through the shock-ionized air surrounding the nose cone.

The vehicle antennas were flush-mounted cavity-backed slots with aperture dimensions of 2.362 x 1.128 in. The cavities were filled with hot-pressed boron nitride, which has a relative dielectric constant of 4. The operating characteristics of this type of antenna are well known and relatively easy to calculate. A sketch of the antenna is shown in Figure 12.

In addition to the microwave system just described, two electrostatic probes were also included as part of the experiment shown in Figure 11. One of these was biased positive, and the other biased negative. The bias potential of both probes was periodically varied throughout the flight. The data collected therefrom (inclusive of others, not part of the experiment in the shoulder region) were also transmitted to the ground via telemetry.

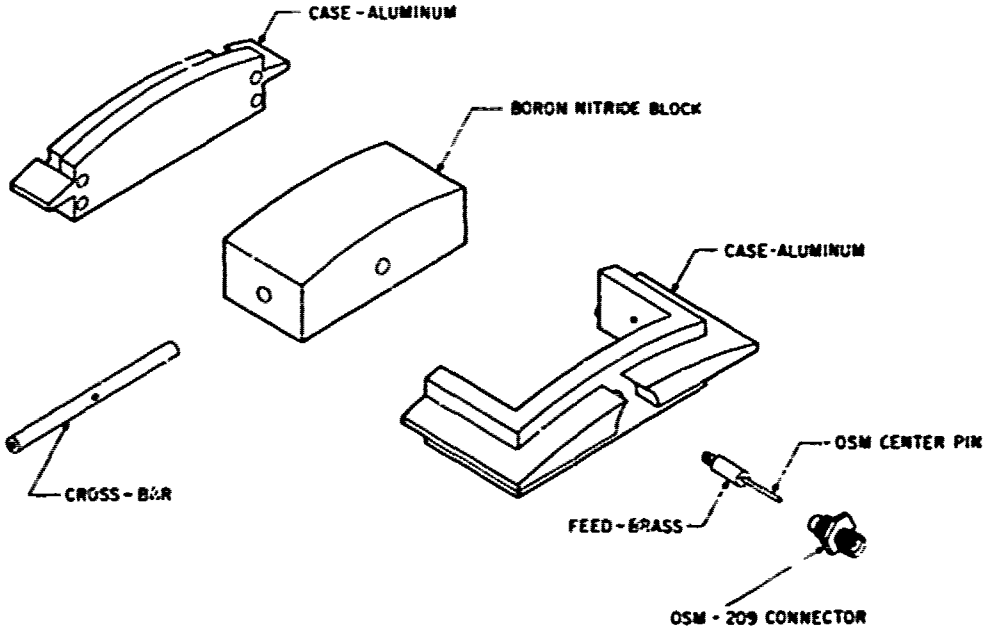

Figure 12. Sketch of S-Band Test Antenna

2.2 Antenna System Performance in a Plasma

The operating characteristics of an antenna can be greatly affected by the presence of a plasma. And almost always, the antenna system—plasma interaction manifests itself as a very significant or catastrophic reduction in the level of the microwave signal received from a reentry vehicle. Signals from external sources are similarly affected before they are received by antennas mounted on reentry vehicles. In addition, there are other effects which though more subtle, nevertheless, lead to equally severe degradations in system performance. Chief among these is the modification of the radiation pattern which is often narrowed when an antenna is covered by a moderately thick plasma slab. Also, the coupling between adjacent antennas is greatly changed. This is of importance in microwave systems employing separate transmitting and receiving antennas, or in multiple aperture antenna systems, where a change in the mutual coupling of array elements can change the over-all radiation pattern. Usually, several of these effects are present simultaneously.

The most direct inflight measurement is that of the power reflection coefficient R, which is related to the magnitude of the antenna impedance mismatch. The reflection coefficient is defined as the ratio of the reflected power P_{ref} to the incident power P_{inc}:

$$R = \frac{P_{ref}}{P_{inc}} . \tag{1}$$

The phase of the antenna impedance can also be determined, but some additional measurements are required. As the plasma density increases, the power reflected from an initially matched antenna also increases. When plasma frequency nears operating frequency, there is a sharp increase in the power reflection coefficient with reflection of most of the incident power. Typical values of R for an overdense plasma are 0.8 to 0.9. The increase in power reflection coefficient is not monotonic, but exhibits small local minima as it nears unity.

Another phenomenon of interest during reentry is the coupling between two adjacent antennas on the vehicle. When the antennas are covered by the plasma, there is a substantial reduction in the power coupled into the receiving antenna P_{rec} from the nearby transmitting antenna, as compared to the free space case. This is due to two causes: The first is the rise in the reflection coefficient of the transmitting antenna, accounting for radiation of only part of the incident power P_{inc}; the second is an increase in the attenuation of the transmitted signal as it propagates to the receiving antenna. Therefore, the interantenna coupling loss (in dB) is defined as

$$\text{Interantenna coupling loss} = 10 \log (P_{inc}/P_{rec}) \tag{2}$$

and includes both internal reflection losses and external attenuation losses. The external coupling loss (in dB) is obtained by subtracting the reflection loss according to the rule:

$$\text{External coupling loss} = 10 \log \left[\frac{P_{inc} - P_{ref}}{P_{rec}} \right] \tag{3}$$

where P_{ref} is the power reflected from the transmitting antenna. The external coupling loss between two S-band slot antennas can be expected to change by 15 or 20 dB.

The increase in attenuation over the free-space value that occurs for a signal propagated from a reentry vehicle to a ground receiving site is important in describing the operation of a microwave radiating system. The signal strength at a point in space depends on the reflection loss due to antenna mismatch, the spatial distribution of the radiated power (antenna radiation pattern), and the attenuation of the signal as it propagates through the plasma. The first of these effects has already been discussed in connection with Eq. (1). It is often difficult to separate the effects of the remaining two properties despite their distinct origins. The signal attenuation is of special concern, if the signal must make a round trip traversal of the plasma as in certain radar applications. But simultaneously, there can be a reduction (or increase) in signal strength because of a plasma-induced modification to the antenna radiation pattern. From a measurement of the power received on the ground P_g and a knowledge of the incident power P_{inc}, the signal attenuation can be found. This quantity relative to its free space value is called the total signal attenuation:

$$\text{Total signal attenuation} = 10 \log \left[\frac{P_{inc}}{P_g} \left(\frac{P_g}{P_{inc}} \right)_o \right]. \tag{4}$$

The term $10 \log \left(P_g/P_{inc}\right)_o$ is the minimum free-space value of the signal attenuation during a complete spin cycle. It is sometimes convenient to define a variant of the total relative attenuation. This alternate form excludes the portion of the signal attenuation that can be attributed to the antenna mismatch loss. Since the antenna is matched to free space, the composite signal attenuation is defined as

$$\text{Composite signal attenuation} = 10 \log \left[\left(\frac{P_{inc} - P_{ref}}{P_g} \right) \left(\frac{P_g}{P_{inc}} \right)_o \right] \quad . \qquad (5)$$

Clearly, these two attenuations depend on the polarization of the signal relative to the receiving antenna, because the actual received power P_g is used in the definitions.

In the case of thin plasmas, there is little change[10] in the radiation pattern and Eq. (4) represents only that attenuation due to the plasma sheath. Otherwise, as for the S-band system of this flight, Eq. (4) represents the total attenuation caused by pattern modification and signal attenuation.

It should be emphasized here that the quantities defined in Eqs. (1) through (5) all depend on the instantaneous position and orientation of the vehicle. The altitude establishes the over-all plasma conditions and the orientation of the nose cone relative to the windward position accounts for angle of attack effects, determining the exact local plasma density. Variations in the antenna radiation pattern of the transmitting antenna and polarization loss depend on the orientation of the nose cone relative to the ground receiving antenna. Therefore, any discussion of particular values of these quantities must include the position and orientation of the vehicle. In the present case, the data are given in terms of a body position (windward or leeward) or the vehicle spin angle ϕ_o for a given altitude.

3. THEORETICAL COMPUTATIONS

3.1 The Ionized Flow Field

The complexity of the interaction between the external plasma flowing around the vehicle and the microwave antennas has been discussed. Several theoretical approaches have been used to describe the electromagnetic phenomena that occur in the presence of an ionized medium. These models require that the electrical properties of the plasma be defined. However, the nature of the experimental conditions makes this a formidable process. In the analysis of a particular antenna result, the ordinary assumption of this report is that the plasma is one-dimensional. This means that the plasma layer over the antenna system varies only in the direction normal to the vehicle surface. In that direction, the models assume that the plasma can be considered as a series of slabs of arbitrary thickness, each characterized by a value of electron density and collision frequency. Thus, for electromagnetic calculations, the required description of the flow field

---

10. Fante, R. L. (1967) Effect of thin plasmas on an aperture antenna in an infinite ground plane, Radio Science 2(NS)No. 1:87-100.

at a location on the vehicle comprises profiles of electron density and collision frequency normal to the antenna surface.

The process of obtaining suitable theoretical profiles during the course of reentry involved numerous calculations. The reentry regime of interest for the Trailblazer II flights extended from around 300 kft down to about 100 kft. Over this range, the atmosphere is quite variable, changing from near free molecular conditions to a well-established continuum regime. Two general altitude divisions were employed for calculations in this report. Below 200 kft, the flow around the vehicle is considered as a two-layer system. Close to the surface is a well-defined thin boundary layer wherein diffusion and viscous effects are important, whereas in the main outer layer, the flow is inviscid. At these altitudes, the chemistry of the flow varies from nonequilibrium to equilibrium as density increases. For the higher altitude regime though, the distinction between the boundary and shock layers is not as precise. Viscous effects are not constrained to occur only at the surface, and the flow becomes highly complex. The gas is in chemical nonequilibrium, and for some conditions even the vibrational modes may not be completely equilibrated. In addition to these general features, nose bluntness effects cause the flow at different vehicle positions to exhibit considerable variability. The nose region is a high temperature ionization zone. Then as the air leaves this area, it expands and cools down so that recombination becomes a dominant chemical process along the afterbody. Vehicle spin and angle of attack effects introduce still further complications. The specific details of the flow calculations for the Trailblazer flights are described by Lennon.[9] In that report, the justifications for extending results from one set of calculations to apply at other conditions are looked into and various limitations described. The emphasis in this report is somewhat different.

The observed plasma effects on the shoulder antennas occurred in a rather narrow altitude range; a number of interesting features were apparent. Analysis, however, required conditions at smaller intervals than the original 20 kft. Therefore, the basic results were manipulated, so that the values for intermediate altitudes could be obtained. Two general sets of data were considered, corresponding to the two reentry regimes of interest. For the cases above 220 kft, the viscous solutions of Lew[11] were selected, whereas while for the lower range, the results of Ball[12] were employed. That the two types of solutions are based

11. Lew, H.G. (1970) Shock Layer Ionization at High Altitudes, AFCRL-70-0702, Final Rpt on Contract F19628-69-C-0112, GE 70SD782, The General Electric Co., Valley Forge, Pennsylvania.

12. Ball, W.H., Webb, H.C., and Lyon, F.J. (1965) Flow Field Predictions and Analysis, Study for Project RAM B3, Space and Information Systems Division Final Rpt No. SID-65-1113, Rpt No. NASA-CR-66106 Contract NAS 1-4743, North American Aviation Inc.

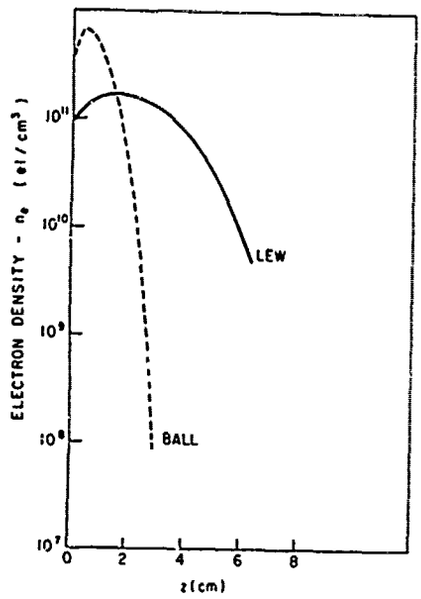

Figure 13. Comparison of Ball and Lew Electron Density Profiles at 215 kft

on vastly different assumptions is emphasized by a consideration of their respective profiles of electron density at the transition altitudes. These are quite dissimilar (see Figure 13).

Both sets of calculations contained profiles of local flow properties and species concentrations. The procedures for interpolation were similar, with results shown in Figures 14 through 17. For each altitude, the electron density was plotted against the normalized distance into the flow z. Then for selected positions along the flow normal, the electron density was replotted as a function of altitude. The species concentrations, pressure, and temperature were used to obtain profiles of the collision frequency. These were then plotted as a function of altitude for selected positions in the flow.

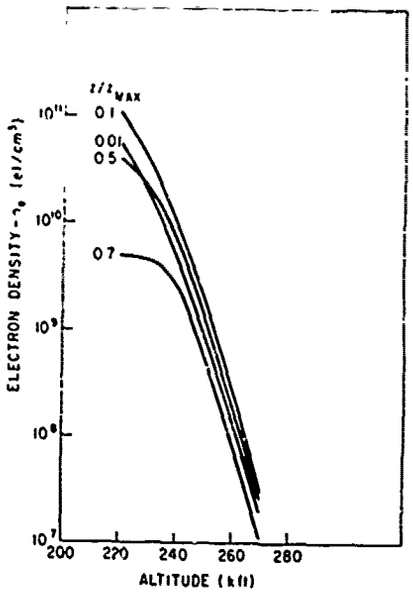

Figure 14. Electron Density Distributions as a Function of Altitude (Lew)

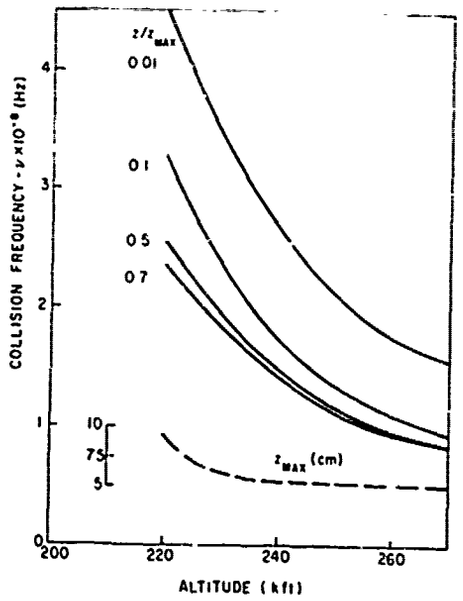

Figure 15. Collision Frequency Distributions and Profile Thickness as a Function of Altitude (Lew)

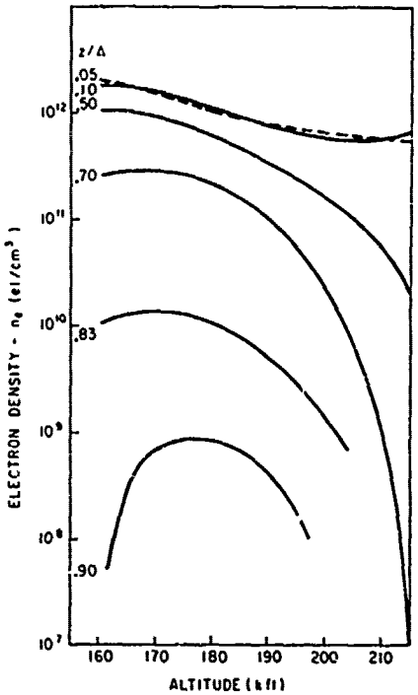

Figure 16. Electron Density Distributions as a Function of Altitude (Ball)

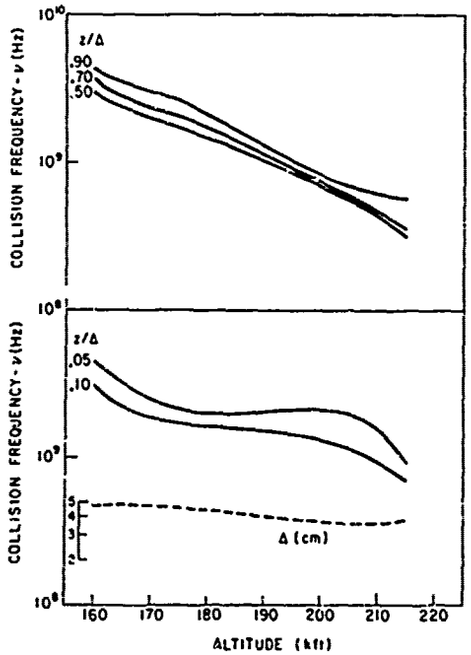

Figure 17. Collision Frequency Distributions and Shock Layer Thickness as a Function of Altitude (Ball)

In the upper altitude regime, a further aspect was considered. In addition to the chemical nonequilibrium, there is also a degree of vibrational nonequilibrium in the molecular species. This alters the flow chemistry and results in changed values for the electron density. The effect is altitude dependent and complex, but it becomes relatively small near 200 kft for the given conditions. A more complete discussion can be found elsewhere.[9] In the stagnation region, a number of these cases were obtained at important altitudes. Peak n_e values for both models were plotted as a function of altitude. By shifting the original equilibrium profiles at those altitudes by the ratio of the corresponding peak n_e values, additional vibrational nonequilibrium cases were then constructed. In the expansion region, the effect of vibrational nonequilibrium was accounted for, by modifying the vibrational equilibrium profiles by a factor corresponding to the ratio of these results in the stagnation region. This represents an upper bound type of approach, since the increased reaction time should result in an over-all decrease in the degree of vibrational nonequilibrium in the flow of the expansion region.

These variations in the models and their effect on the electromagnetic properties will be discussed further, upon comparison of the results.

3.2 Antenna Parameters

Once the flow fields have been specified, the effect of the covering plasma slab on the performance of an antenna is calculated by three different procedures: The first analysis includes the complete specification of all antenna parameters of interest; the other two are plane-wave approximations of differing levels of sophistication. These give reflection coefficient and signal attenuation only. A brief description of these methods will be presented here. A comparison of the results will be made in Section 4, including agreement with the flight data.

The first method of obtaining the theoretical antenna parameters involves the use of a computer program developed by Fante.[13] This program considers a pair of slot apertures, mounted in an infinite ground plane, radiating through an inhomogeneous plasma. The quantities computed are the aperture admittance of the slots, the inter-antenna coupling and the net signal attenuation including antenna pattern modification. From this and the physical characteristics of the antenna, the terminal impedance is obtained. Calculations[14] show that this flat plate model closely approximates the radiation properties of the shoulder antennas on the Trailblazer II.

Because of the steepness of the Trailblazer II trajectory, the diameter of the nose cone relative to the wavelength, and the broad beamwidth of the antennas, certain simplifying assumptions can be made. Specifically, the nose cone can be replaced by a cylinder descending in a vertical trajectory and the cylinder so far as the calculation of the radiated fields is concerned can be replaced by an infinite ground plane. With these assumptions, the Fante program describes the antenna fields (relative to the antenna aperture) in terms of a spherical-polar coordinate system indicated in Figure 18. Here, the aperture is in the x-y plane, the z axis is normal to the antenna, the polar angle is limited to $\pi/2$ radians, and the origin of this coordinate system is in the center of the aperture. Since only the fields far from the antenna are of interest, it is possible to represent the origin as being on the central axis of the nose cone. The y axis of the antenna coordinate system is then coincident with the spin axis of the reentry vehicle. The motion of the vehicle is introduced by allowing the antenna coordinate system to rotate about another fixed system (x', y', z') which locates the nose cone. As shown in Figure 19, the

---

13. Fante, R. L. (1971) Reentry Antenna Test Program, Vol. 2, AVCO System Division Rpt AVSD-0374-69-CR.

14. Poirier, J. L., Antonucci, J. D., and Tropea, D. H. (1973) Performance of a Microwave Antenna System in the Shoulder Region of a Blunt Reentry Nose Cone, AFCRL-TR-73-0656.

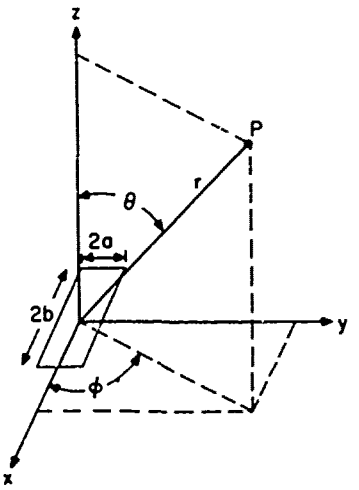

Figure 18. Coordinate System for Slot-Antenna Radiation Fields

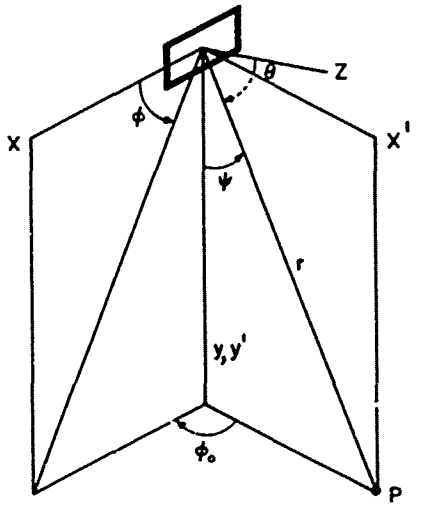

Figure 19. Coordinate Systems for Reentry Nose Cone and Shoulder Antenna

y and y' axes are coincident, r is the distance from the antenna (nose cone) to the ground receiving site in the primed system, the spin angle ϕ_o measures the rotation between the two coordinate systems, and ψ is the local look angle. Because the reentry is vertical, ψ is fixed for many rotations of the nose cone and varies so slowly with altitude that it can be considered constant and equal to 59 degrees for all altitudes between 250 and 200 kft.

In this program the plasma is modeled in terms of a series of uniform dielectric slabs covering the two antennas. The particular thickness chosen for these slabs depends on the electron density distribution normal to the vehicle surface. Each slab is characterized by a representative electron density and collision frequency which establish the effective dielectric constant for use in the program. Typical input values of electron density, collision frequency, and slab thickness are shown in Table 3. These cases represent the basic vibrational equilibrium calculations for the expansion region.

From these plasma properties and the physical characteristics of the transmitting antenna, the signal attenuation was computed as a function of ϕ_o for each altitude of interest. The results for $\psi = 59^o$ are shown in Figure 20. These two sequences of curves require some explanation before discussion of the various models is continued. The attenuation which is shown refers to the reduction in the power (relative to the maximum free space value) observed by a completely polarized receiving antenna on the ground. The variation in the free space value

Table 3. Plasma Layers Derived from Electron ısity and Collision Frequency Profiles at Four Altitudes

Altitude (kft)	Slab Thickness (cm)	Electron Density $n_e \times 10^{-10}$ (el/cm^3)	Collision Frequency $\nu \times 10^{-8}$ (Hz)
240	0.10	0.41	3.37
	0.19	0.76	2.49
	0.29	0.96	2.15
	0.37	1.08	1.90
	0.42	1.12	1.77
	0.46	1.07	1.74
	0.49	0.84	1.71
	1.35	0.59	1.67
	0.78	0.19	1.58
	0.72	0.03	1.56
235	0.29	1.00	3.01
	0.84	2.10	2.00
	1.12	2.25	1.83
	1.12	1.40	1.68
	0.56	0.38	1.60
230	0.32	1.90	3.44
	0.88	3.90	2.35
	1.22	3.90	2.10
	1.22	2.20	1.93
	0.61	0.45	1.83
225	0.37	3.40	3.91
	1.03	6.80	2.75
	1.42	6.60	2.44
	1.42	3.10	2.22
	0.71	0.48	2.08
220	0.55	9.00	3.50
	0.75	11.00	3.25
	1.00	11.00	2.95
	1.00	9.60	2.80
	1.00	6.30	2.60
	1.00	2.75	2.50
	1.00	0.84	2.40
	1.00	0.15	2.30
	1.00	0.01	2.30
215	0.48	9.00	5.00
	1.32	16.00	3.85
	1.82	14.50	3.30
	1.82	4.60	2.96
	0.91	0.48	2.65

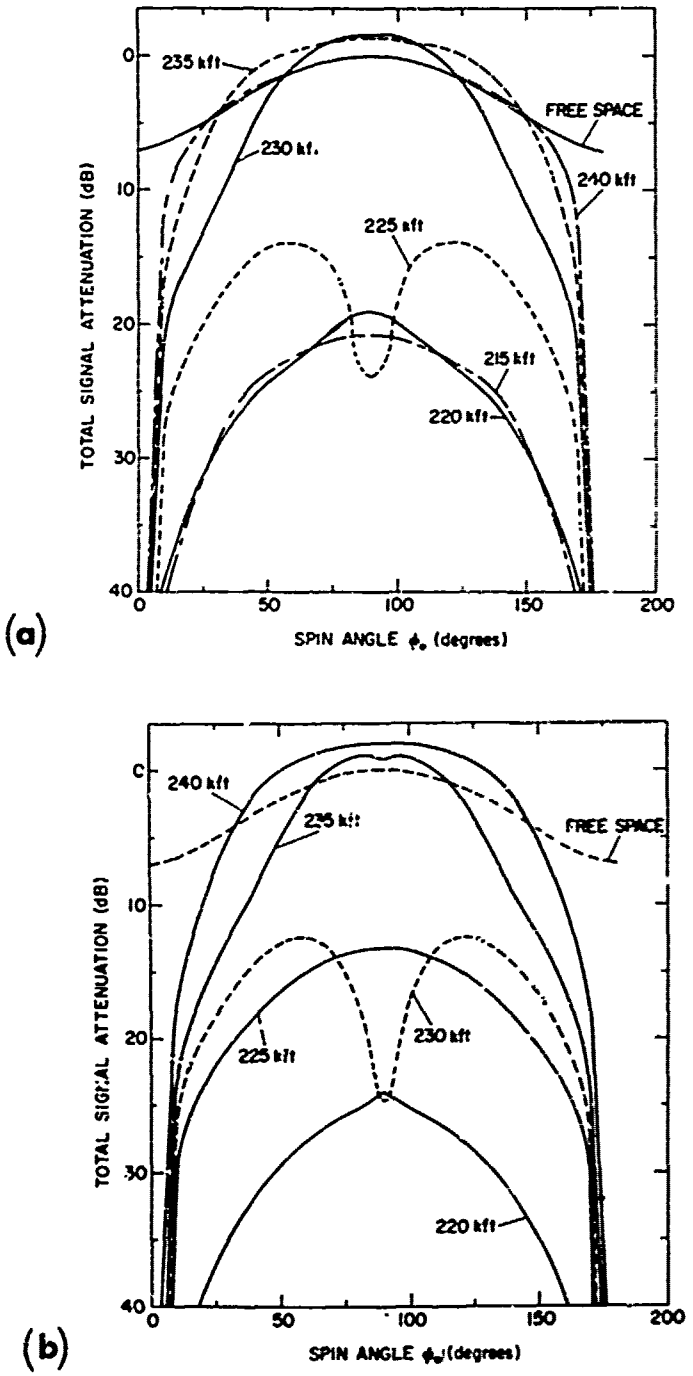

Figure 20. Calculated Total Signal Attenuation at Various Altitudes: (a) vibrational equilibrium model; (b) vibrational nonequilibrium model

is also plotted for comparison. The results in part (a) are based on vibrational equilibrium plasma properties while in part (b) similar curves are shown for the theoretical profiles modified to show the effect of vibrational nonequilibrium. The general effect of increasing ionization is to narrow the patterns while simultaneously increasing the over-all level of attenuation. Both sets indicate a resonance phenomenon. This condition is critically dependent on the local plasma properties and the signal path length appearing at 225 kft for the vibrational equilibrium input but at 230 kft for the vibrational nonequilibrium set. Allowing for this mechanism in the flow model tends to increase the electron concentration levels at a given altitude. This effect is carried over into increased attenuation; for instance, at 220 kft the vibrational nonequilibrium curve shows 5 dB more attenuation. These results will be examined in more detail in the next section.

The plane wave models do not allow for a power pattern in their calculations, and so their single-valued results will be deferred until the section on comparisons. For the simpler of the two plane wave approximations, attenuation and reflection estimates were made along the lines indicated by Russo.[15] The variation of the attenuation constant along the normal to the antenna is first determined. An integration is then carried out over this distribution to obtain the signal loss in the plasma medium (in dB) due to attenuation,

$$(SL)_A = 8.686 \int_0^{z_{MAX}} \alpha \, dz \quad , \tag{6}$$

where α is the local attenuation constant, which is related to the values of the dielectric constant for the plasma slabs.

For the reflection, an equivalent slab thickness associated with the peak α value is then determined:

$$d_E \equiv \left(\int_0^{z_{MAX}} \alpha \, dz \right) \Big/ \alpha_{MAX} \, . \tag{7}$$

The peak attenuation constant α, its corresponding phase constant β, and the effective thickness d_E then serve to specify the reflection coefficient:

$$R = \frac{R_{12}\left[(1-e^{-2\alpha d_E})^2 + 4e^{-2\alpha d_E} \sin^2 \beta d_E \right]}{(1-R_{12}e^{-2\alpha d_E})^2 + 4R_{12}e^{-2\alpha d_E} \sin^2(\delta_{12}+\beta d_E)} \quad , \tag{8}$$

15. Russo, A.J. (1963) Estimates of Attenuation and Reflection of Telemetering Signals by Ionized Flow Fields Surrounding Typical Reentry Bodies, NASA Technical Note TN D-1778.

where R_{12} is the power reflection coefficient for a uniform semi-infinite plasma and δ_{12} is the relative phase difference. This can be converted from a coefficient to a reflection loss (in dB) term as was done for the attenuation:

$$(SL)_R = 10 \log_{10} \left(\frac{1}{1-R} \right) . \quad (9)$$

The degree of approximation is severe, and many factors such as internal reflections are not included in these relations. The results are, nevertheless, quite good, except that resonance effects for both attenuation and reflection do not occur.

The second of these models came from a formulation originally developed for a different situation. Papa[16] has studied the interaction of electromagnetic waves and ionized reentry flows for high power signal strength. His calculations were based on a number of high altitude reentry conditions for the Trailblazer II vehicle. Since his theory could be applied to the case of low power transmission as well, some typical cases were computed for comparison with the other calculations. Papa's approach involves numerical solution of the electron continuity equation to determine the field distribution and power transmitted through a one-dimensional plasma slab with specified profiles of fluid and electrical properties. Since the electric field is determined on a point by point basis, internal absorption and reflection are included, and the result should be quite exact. The numerical procedures rely on a fourth-order Runge-Kutta technique for integrating the equations across the slab, and the small step size restricts the error to no greater than 0.006 percent. This solution then represents an extremely reliable check of other plane wave results. In addition, the Fante result for a case where the antenna aperture dimensions are changed so that they are several wavelengths in extent (producing what is effectively a plane wave condition) also should be in close agreement.

4. FLIGHT TEST DATA AND COMPARISONS

In this section, the measured flight test data will be presented and compared with computed results from various models for the flow field ionization. The antenna properties to be considered are: signal attenuation pattern modification, impedance mismatch as characterized by the power reflection coefficient, and interantenna coupling.

---

16. Papa, R.J. and Taylor, R.L. (1974) High-Power electromagnetic transmission characteristics of a diffusing reentry plasma, J. Appl. Phys. 45 (No. 2):684-696.

Measurement of the signal attenuation pattern requires that the signal strength received on the ground be determined as a function of vehicle spin angle throughout the reentry trajectory. This is accomplished by recording the receiver age voltages which showed one main lobe. The back lobe, however, was not evident even at altitudes sufficiently high to ensure that no ionization effects yet existed. This distortion was introduced by the ground station receivers, because the frequency response of the age loop was too low to follow antenna pattern variations of the spinning vehicle. This loss of data in the back lobe region is not significant in so far as the present study is concerned, since the theoretical models either employ a plane wave, or else consider the slot aperture to be mounted on an infinite ground plane. Neither approach considers radiation in the backward direction, so comparisons could not be made there in any case.

There is yet another consequence resulting from the use of a flat-ground plane model in which the antenna is covered by a plasma slab of infinite lateral extent. Reference to Figures 18 and 19 will help to visualize the geometry of the model for $\phi_o = 0^o$. In this case, the plasma slab extends all the way to the ground-receiving site and the propagation path is wholly within the plasma. As ϕ_o increases sufficiently, the propagation path extends across and beyond the slabs, and flight conditions are more accurately simulated. Because the model predicts far too much attenuation at grazing angles, the comparison of results should be limited to spin angles $10^o < \phi_o < 170^o$.

The observed data at an altitude of 230 kft were used in Eq. (4) to compute the total signal attenuation, with results plotted in Figure 21. The received power was obtained as a function of spin angle from the age records, and the factor $(P_g/P_{inc})_o$ evaluated by noting the peak value of the received signal just before reentry. Inspection of this figure shows that there is reasonably good agreement between the computed value (vibrational equilibrium) and the measured curve. In contrast, there is a marked discrepancy between the measured data and the vibrational nonequilibrium values which, in fact, show a resonance at this altitude.

The same quantities are plotted in Figure 22 for an altitude of 225 kft. At this altitude, the maximum value of attenuation predicted by the two models is about the same and the maximum variation at $\phi_o = 90^o$ is only about 10 dB as compared to 25 dB for the previous case (230 kft). The vibrational equilibrium pattern now shows a resonance, as does the curve of measured values.

At both altitudes, the two calculated attenuation values for $\phi = 90^o$ are the result of the resonance phenomena. As discussed in Section 3.1, the vibrational nonequilibrium results represent an upper bound on the expansion region electron density, which should be less applicable as the altitude decreases. Thus it is not surprising that the nonequilibrium calculation shows the resonance at a higher altitude than both the equilibrium calculation and the measured values.

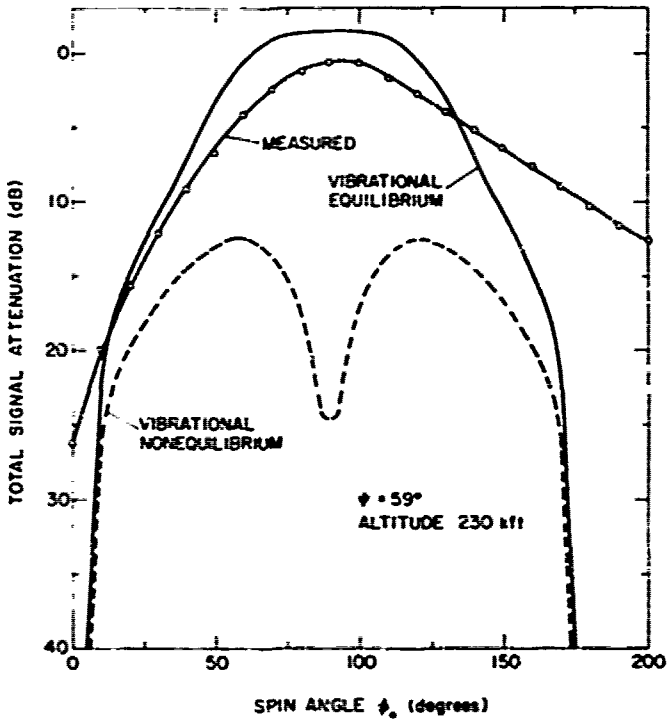

Figure 21. Total Signal Attenuation Comparisons at 230 kft

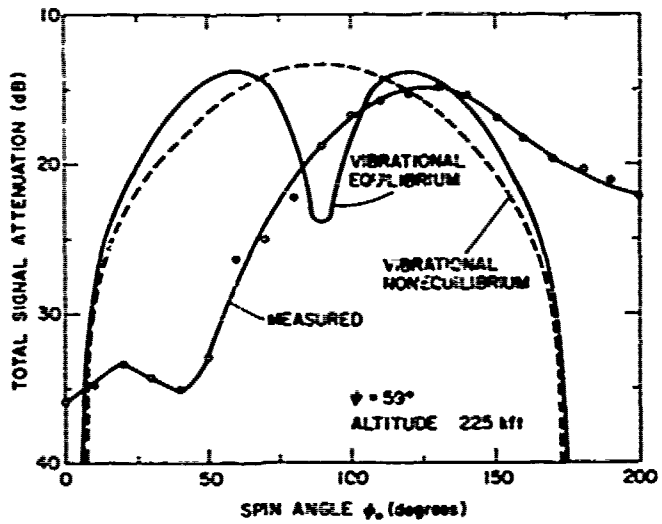

Figure 22. Total Signal Attenuation Comparisons at 225 kft

The resonance occurs over a very narrow altitude range (about 3000 ft). The theoretical calculations assume constant properties during a spin cycle, whereas in flight a change of about 1.5 kft altitude occurs during one revolution, altering the local plasma seen by the antenna. Thus the important fact here is not the differences between the two models, or the altitude where the resonance occurs, but rather the fact that the predicted resonance was indeed observed despite the variation in conditions experienced by the antenna.

At altitudes below 220 kft, the Ball description of the ionization becomes more appropriate. The computed attenuation pattern for this model is compared to the measured pattern for an altitude of 210 kft in Figure 23. The over-all narrowing of the patterns is evident but there is a 10-dB difference between the peaks of the two curves.

The transition between the two sets of calculations[12] however, is not completely straightforward. Figure 24 shows the attenuation from both models and the observed pattern at 215 kft. The curve for the Ball model is clearly in better agreement with measured results than the Lew profile, which represents a downward extrapolation of the results at higher altitudes. Note though that the Ball results at 210 kft are in poorer agreement with the corresponding observed values than for the 215 kft case. Thus the pattern is not completely consistent, and some care must be taken.

The observed attenuation patterns involve the orientation of the vehicle-ground receiver system. This introduces a further degree of uncertainty: The vehicle enters at an angle of attack, and although its location with respect to the ground station is known as a function of time, the orientation of body axis to flight path is continuously changing. Thus its position at a given moment is unknown and cannot be specified precisely. This nonalignment results in the flow being three-dimensional, introducing an additional plasma profile variation in the spin plane. A second aspect involves the alignment of the vehicle axis with the ground receiver. The power distribution obtained during a spin cycle will not be symmetrical unless this additional alignment corresponds to a windward or leeward orientation of the vehicle. For a windward condition, the peak signal strength would be less than for the leeward alignment, but for both, the pattern would be symmetrical about the peak. Any other orientation results in an asymmetric pattern, that is, if the alignment represents a condition midway between windward and leeward, the measured attenuation for some ϕ_o such that $0^o < \phi_o < 90^o$ would be greater or less than for its corresponding angle in the range $90^o < \phi_c < 180^o$. This effect cannot be seen in the computed patterns, since they are based on the assumption of a plasma that is uniform, except in the normal direction.

Since the flight data is to be compared with theoretical results, losses in signal strength due to reflection are included in the over-all observed losses

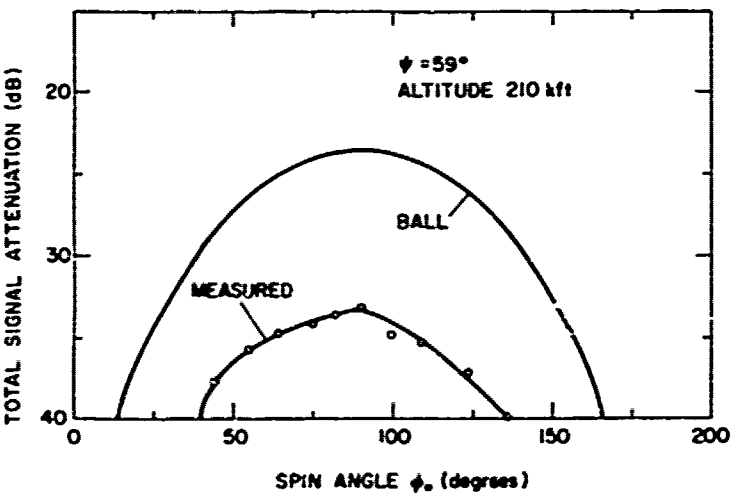

Figure 23. Total Signal Attenuation Comparisons at 210 kft

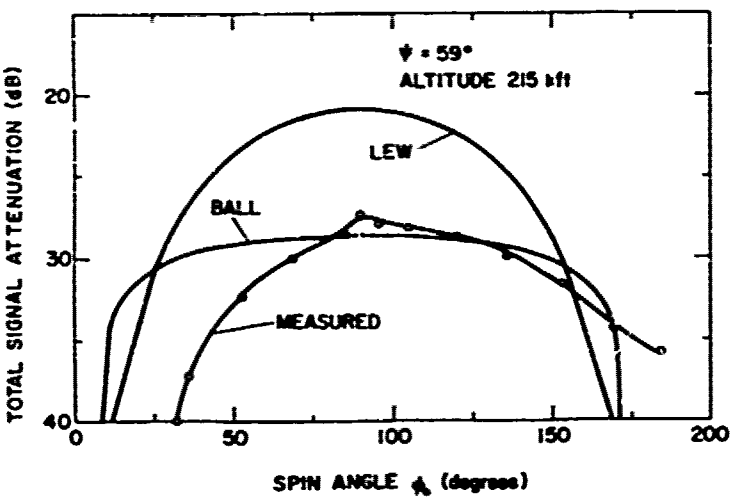

Figure 24. Lew and Ball Results for Total Signal Attenuation at 215 kft

plotted in the figures. This was done since there is some difficulty in separating that effect in the calculations. Since the flow ionization is not axisymmetric, the antenna reflection losses and power pattern distributions in the course of a spin cycle contain a degree of ambiguity. Some bounds can be placed on this for the reflection case. The limit of the uncertainty is the difference in reflection losses for windward and leeward conditions. Its magnitude depends on the plasma properties and hence varies as a function of altitude. This is shown in Figure 25. The profile indicates the earlier increase in the plasma on the windward side, the region where the entire flow is overdense, and some subsequent structure.

Several properties are independent of ground reception. An important one is the power reflection coefficient R. The measured values corresponding to the leeward and windward body axis positions are plotted in Figure 26. Inspection of these curves shows that during the plasma buildup R was always larger on the windward side than on the leeward side. This variation gradually diminished as the electron density levels increased. Below 180 kft, the plasma was overdense during the entire spin cycle, resulting in a uniform degree of reflection at all times. An interesting feature of the plasma build-up period is that the reflection coefficient did not increase monotonically but exhibited a local minimum. Two theoretical curves are also plotted in this figure. One computed from the vibrational equilibrium model also exhibits a small local minimum near the peak of its excursion. The curve for vibrational nonequilibrium shows a much larger local minimum occurring at a higher altitude. This curve is in better agreement with the windward values initially but it greatly overestimates R at lower altitudes.

The measured values for the reflection coefficient are compared to values computed with the simplified equivalent slab plane wave method in Figure 27. Several descriptions of the ionization properties were used for various altitude ranges, and the over-all trend for the observed R values is followed by the calculations, including the decrease in plasma effects at the lower altitudes. Again, during plasma buildup the vibrational nonequilibrium model gives better agreement with observation. There is a slight underestimation of the plasma, but the slope of the rise is similar and the values correspond to within 10 kft. The coupling between the two shoulder antennas, defined by Eq. (2), is plotted in Figure 28 for the leeward and windward sides. As was true for the power reflection coefficient, the effect of the plasma on the interantenna coupling was greater on the windward side. Due to limitations imposed by the sensitivity of the measuring system, the curves for the observed windward and leeward interantenna coupling are terminated below 200 kft. The measured coupling remained below 37.5 dB for the remainder of the flight. The curves also show that the decrease in coupling was not monotonic but exhibited several local maxima as well as a

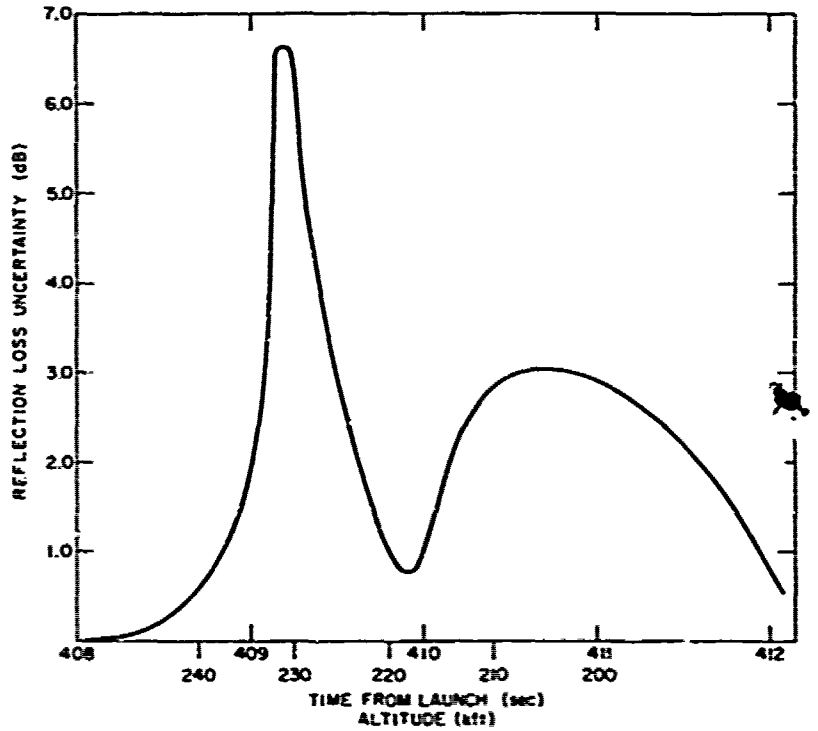

Figure 25. Variation in Reflection Loss During a Spin Cycle as a Function of Altitude

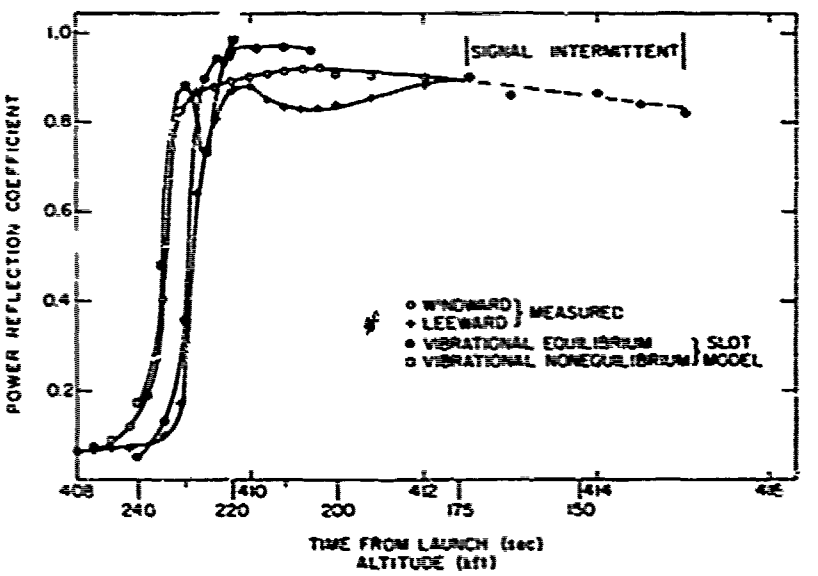

Figure 26. Comparison of Slot-Antenna Reflection Coefficient with Flight Data as a Function of Altitude

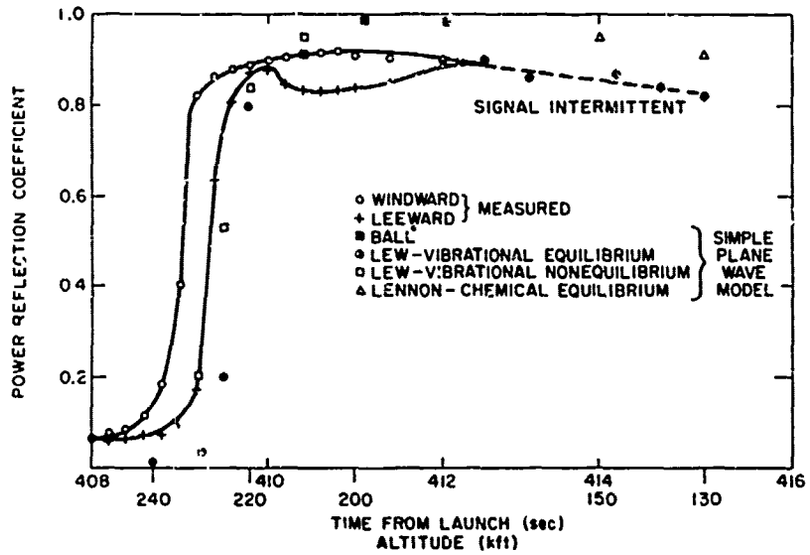

Figure 27. Comparison of Plane Wave Reflection Coefficient with Flight Data as a Function of Altitude

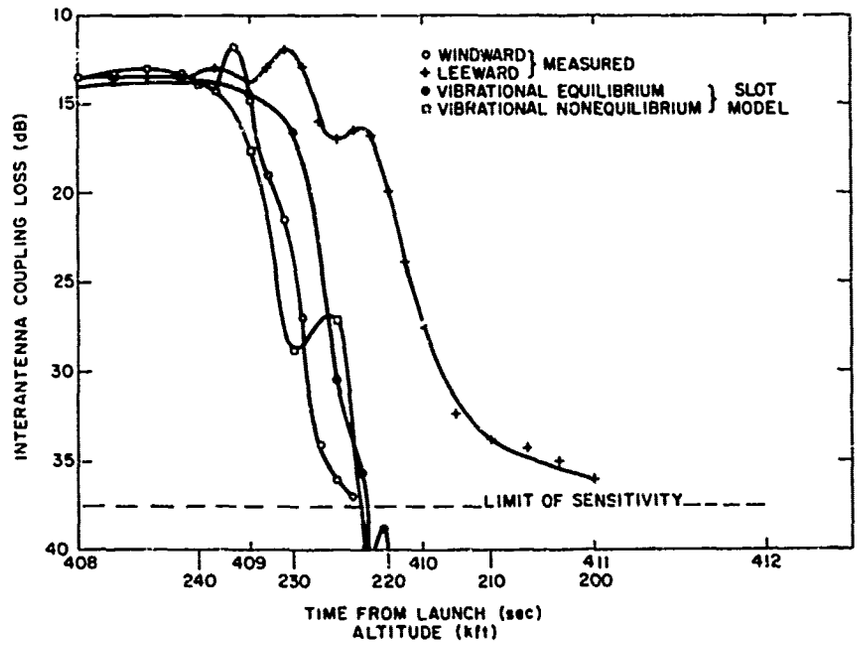

Figure 28. Comparison of Calculated Interantenna Coupling with Flight Data as a Function of Altitude

slight increase at plasma onset. The computed values for vibrational nonequilibrium and equilibrium conditions are also shown in Figure 28.

Both models tend to follow the windward observed values. Since the vibrational nonequilibrium results represent an overprediction of the zero angle-of-attack ionization levels, it is not surprising that it would be closer to that curve. Both models also predict some local maxima, although their values for the coupling at these extremal points differ considerably from the corresponding flight data.

The observed attenuation patterns at selected altitudes have already been discussed, as well as the corresponding theoretical patterns from the Fante model. In order to examine trends and make comparisons with the plane wave calculations, some additional consideration must be given to the altitude history of those results, as was done for the reflection and coupling cases.

The procedure for obtaining the flight profile consisted in plotting the attenuation at constant $\phi_o = 90^o$ as a function of altitude. These values are shown in Figure 29 along with the Fante theoretical curves. For example, the local maximum which occurs in the curve based on the vibrational equilibrium model was

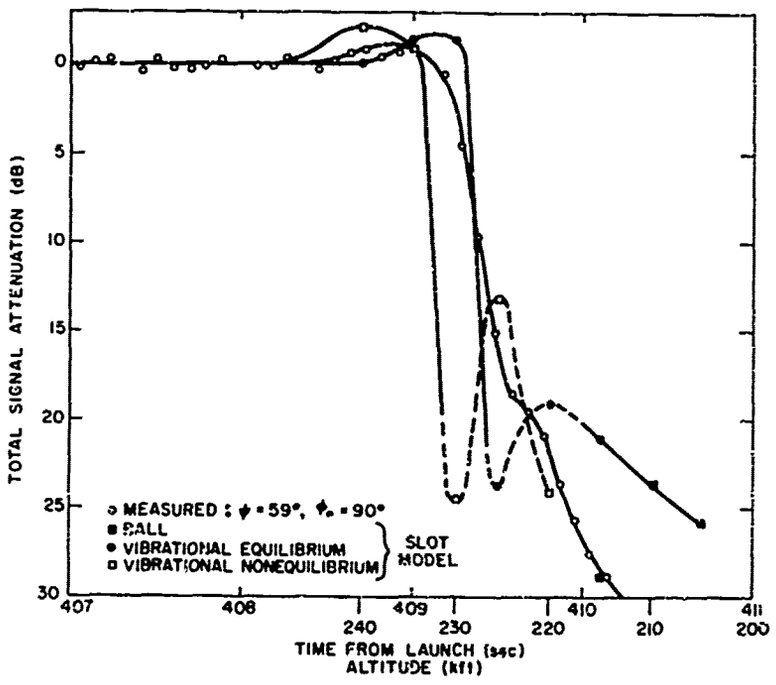

Figure 29. Comparison of Slot-Antenna Total Signal Attenuation with Flight Data as a Function of Altitude

taken from the 225-kft curve of Figure 20a, evaluated at $\phi_0 = 90^\circ$. The effect of the resonances which appear in Figures 20a and 20b is graphically illustrated by this construction. The general shape of the computed curves first shows a slight decrease in attenuation caused by increased gain of the transmitting antenna and then a rapid increase in attenuation interrupted only by a local maximum. The assumption of vibrational nonequilibrium causes the resonance to occur at a higher altitude, but the over-all profiles are similar. The measured data agree generally with the computed values, showing a decrease in attenuation at plasma onset and a hump characteristic of a small resonance effect at about 223 kft. There is some disagreement between measurement and observation at the low altitudes. Although the uncertainty in reflection loss might account for a factor of 1 or 2 dB, there is still a definite underprediction of the losses below 220 kft.

The measured signal attenuation and the one computed using the simplified plane wave method are compared in Figure 30. In this comparison, the non-equilibrium values show better agreement with experiment as far down as 220 kft in altitude.

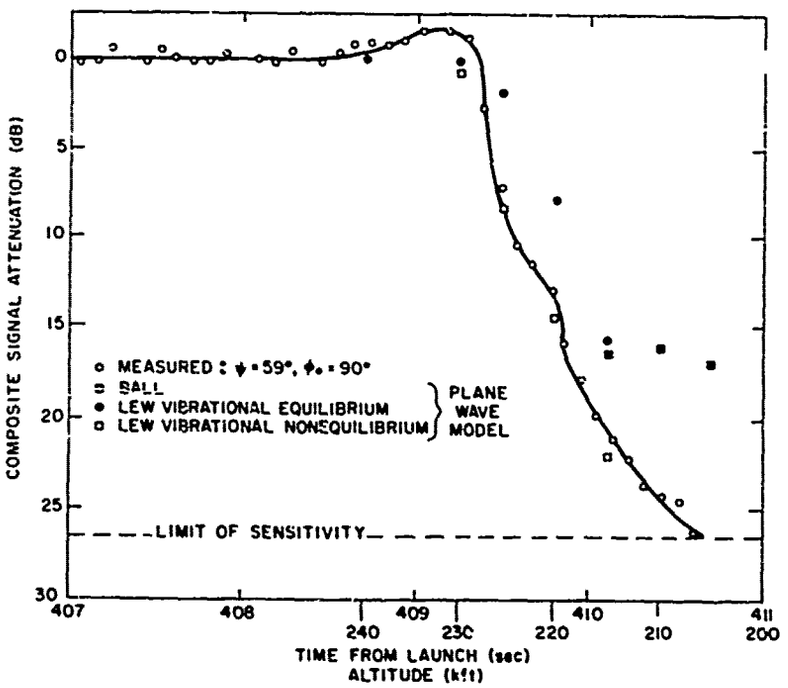

Figure 30. Comparison of Plane Wave Total Signal Attenuation With Flight Data as a Function of Altitude

The slight rise near plasma onset and the peak at 225 kft are not apparent in this plane wave result. This is probably attributable to the lack of internal reflection losses and the inability of the model to account for variations in antenna gain. Again, below 220 kft the predicted values begin seriously to underestimate the losses. Despite the good agreement over most of the rise portion, the slot-antenna model with the assumption of vibrational nonequilibrium, has better over-all correspondence with the complete profile including resonances.

There is another factor which must be considered when the attenuations predicted by the two models just discussed are compared. This new factor arises because the propagation path length in one model may not be equal to that in another. All the theories assume the plasma medium to consist of a stack of semi-infinite slabs. But while the plane wave models consider a wave propagating in the normal direction, the Fante slot model was evaluated for a local look angle $\psi = 59^{\circ}$. This means that the propagation path is greater in the latter model which, therefore, should predict more attenuation. This can, in fact, be seen by inspecting the computed curves in Figures 29 and 30. The path length, though, should not seriously affct the reflection as long as the peak n_e value is sufficiently high.

A direct comparison between the two attenuation results can be obtained by evaluating the slot model for a local look angle of $\psi = 90^{\circ}$. The results of these calculations are shown in Figure 31 (circles connected by solid lines). This figure is designed to compare broadside transmission models. Thus it also contains results for the simple plane wave method (solid and open squares) corresponding to those of Figure 30. There is excellent agreement between the two models, but the drastic differences in their basic assumptions suggest that this might be fortuitous. In particular, Fante's slot model includes the effect of multiple internal reflections at each plasma slab interface, while this plane wave model does not. Thus the latter should predict lower values of attenuation, since no energy is scattered back toward the source. On the other hand, the increase in peak gain of the transmitting antenna in the Fante model may serve to offset the expected difference.

In order to study this problem in more detail, two additional sets of calculations were made. The first consisted in allowing the aperture dimension in the slot model to become larger, so that the antenna would launch a wave that would more nearly approximate a plane wave. The results of this exercise are plotted as triangles. The other, based on Papa's work, assumes a plane wave solution but includes internal reflections at slab interfaces. These points are plotted as upside-down triangles. Inspection of these two sets of results shows that they are in close agreement with one another, as expected. Note that below 220 kft though, they are quite different from the simple plane wave and narrow aperture

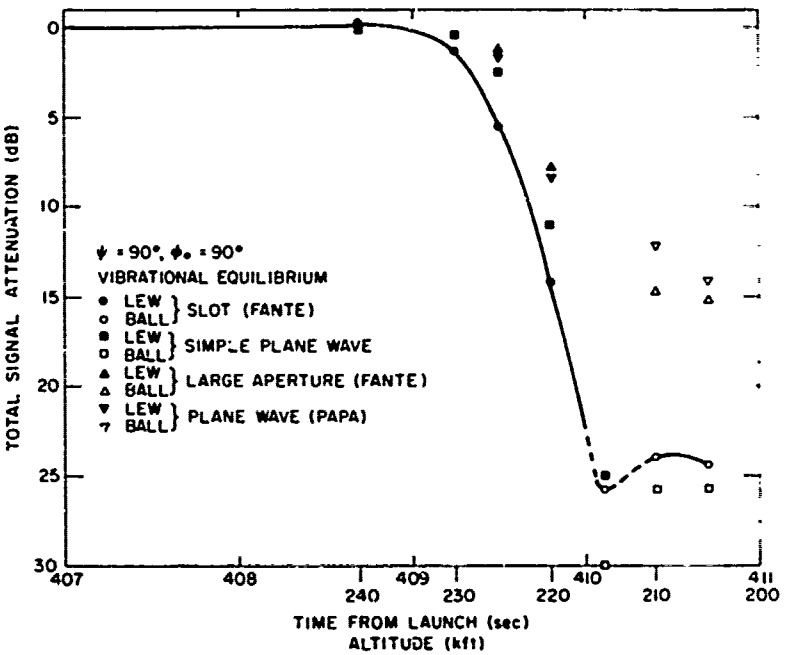

Figure 31. Peak Total Signal Attenuation as a Function of Altitude for Various Theoretical Models

slot results. This confirms the anticipated conclusion that the agreement between the simple plane wave and slot approaches represented a balance of compensating theoretical factors. It should be pointed out that the new results below that altitude are even less in agreement with the observed data.

To complete the comparison of the four methods, the power reflection coefficient corresponding to every data point on the attenuation curves of Figure 31 is plotted in Figure 32. As can be seen, there is a significant spread in the results predicted by these various models. If the excellent agreement between the slot reflection results and the observed data in Figure 26 is recalled, there are a number of comments that can be made. The simple plane wave consistently underpredicts the level, presumably due to the neglect of internal reflections which have an important effect during buildup. Once the plasma has become sufficiently overdense though, the high reflection near the antenna reduces the differences among the plane wave approximations. The fact that the narrow aperture slot results are higher than all the others, suggests that the power distribution may be important.

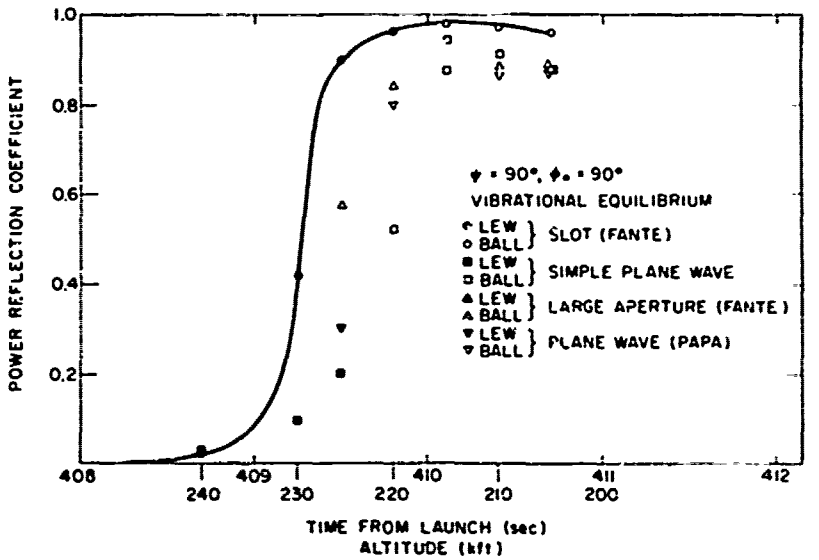

Figure 32. Power Reflection Coefficient as a Function of Altitude for Various Theoretical Models

The effect of power pattern distribution on the total peak attenuation for the slot antenna model has been discussed in some detail. The dependence on look angle ψ was also brought out by the results obtained for the plane wave comparisons. Those results showed considerable change in power pattern structure compared to the case for $\psi = 59^{\circ}$, indicating that the peak electron density level was not the only determining factor in producing the distinctive variations in pattern at various altitudes. Clearly, the local path length in the medium has a strong contribution. To develop this point, an intermediate look angle case ($\psi = 75^{\circ}$) was considered in addition to the cases for $\psi = 59^{\circ}$ and $\psi = 90^{\circ}$. The three altitude histories of peak attenuation are shown in Figure 33. For a given plasma profile normal to the antenna, the variations in path length produce distinctly different attenuation results for some of the conditions.

Two different types of data presentation have been used: The distribution of power for various spin angles at successive altitudes; and the peak attenuation for each altitude at various look angles. In each case various local resonances, or abrupt changes in trend are apparent. Typically, these effects are of short duration, since flight conditions are changing rapidly at these altitudes. Both types of display are important, since they act to clarify each other in delineating an extremely complex sequence of results. For example, the resonance in total signal attenuation observed at 225 kft with $\psi = 59^{\circ}$ was not present in the other

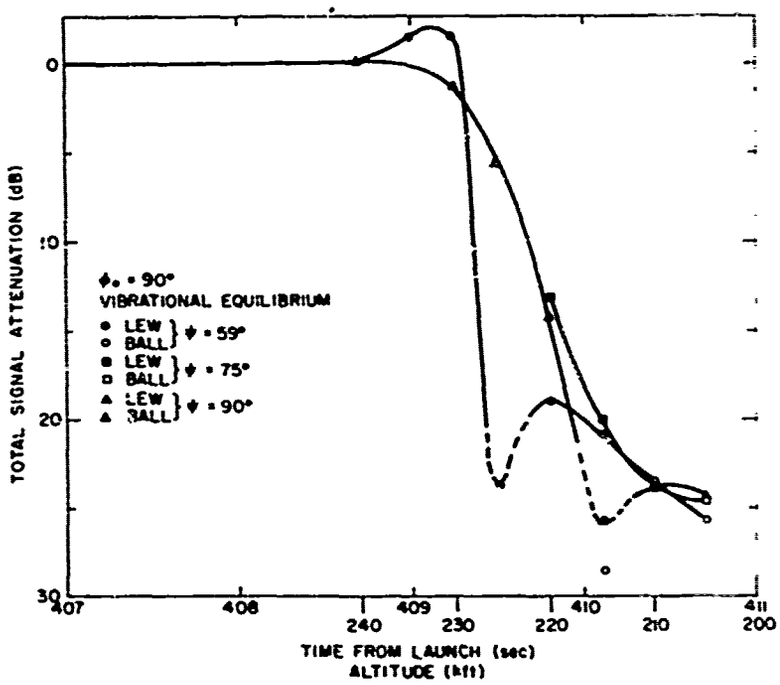

Figure 33. The Altitude History of Slot-Antenna Total Signal Attenuation for Various Look Angles

altitude plots for that look angle or in the results at that altitude for $\psi = 75^{\circ}$ or $\psi = 90^{\circ}$. In the same manner, the peak attenuation curves of Figure 33 show local resonances for $\psi = 59^{\circ}$ and $\psi = 90^{\circ}$ at different altitudes. Combining both types of results leads to the conclusion that these various resonances correspond to a narrowing of the radiation pattern of the antenna for those particular local conditions. Thus the resonances are critically dependent on the interrelation of look angle, electron density concentration, and path length.

The comparisons of the flight test antenna data and the various theoretical methods and flow models have been presented in detail. There are a few aspects which may be placed in perspective by some further discussion. However, these topics do not represent a single clear subject but range from limitations of the assumptions to interpolation in the flow profiles.

The slot-antenna model should be expected to give the most reliable results, but it is restricted by the assumption of ground plane rather than vehicle mounting. The additional constraint of relying on inputs of electron density and collision frequency profiles, as well as the assumption of uniform semi-infinite plasma layers, also limit the agreement with the data. The point by point distribution

of power in the antenna pattern also seems to be an extremely sensitive factor, playing an important role in determining signal losses. The problems of this sensitivity were demonstrated clearly, when the broadside results were duplicated at a number of altitudes with an increased aperture size. At 220 kft, for example, this change decreased the peak attenuation from 23.6 dB to 17.2 dB and the reflection coefficient from R = 0.96 to R = 0.84.

Scaling and interpolation as well as the use of different flow models all had an effect on the theoretical predictions. In general, the basically different assumptions of the Lew and Ball models meant the profiles were not at all alike and the results quite different, as was seen in the region where the transition was employed. The results for the Ball model down to 200 kft seemed somewhat erratic in agreement and tended to underestimate the losses. In the Lew case, the two conditions of vibrational equilibrium and nonequilibrium were both employed. The extrapolation of the latter model from the stagnation region was crude and represents an upper bound rather than actual expected value. Note that the decreasing altitude results should be poorer, since the increased density in the flow would tend to restore the equilibrium sooner for those cases. It should be kept in mind that all these profiles are based on axisymmetric flow assumptions (angle of attack, $\alpha = 0^{\circ}$). The flight had a large value of α, and this certainly affected the results. That the results on the windward side appear to be in better agreement is based on the fact that the flow is still close to the axisymmetric case at the antenna location, whereas corresponding leeward results show considerable three-dimensional flow characteristics. The windward condition for the angle of attack situation would result in an increased shock strength at the antenna location with higher electron density levels across the flow profile.

In the various attempts to match the rapidly changing antenna results, it became apparent that phenomena were occurring in extremely short altitude ranges and that the use of some form of interpolation would be necessary. In order to check on the validity of scaling based on ratios of peak n_e, both scaled and constructed profiles at 224 kft were entered into the antenna program. The agreement was excellent: the peak attenuation values were 61.6 dB and 62.3 dB whereas the reflection coefficient R = 0.91, remained unchanged. In all the scaling techniques, the collision frequency is assumed to be insensitive to the slight changes in conditions, it is held constant at its original value.

The simple plane wave approach is the most severely limited technique. Its restrictions on the plasma and its assumed equivalent slab for calculating the reflection do not take into account internal reflections. Although this eliminates much of the ability to predict fine structure, this model was adequate in terms of producing equivalent profiles for the antenna properties although displaced in altitude. These calculations for the present expansion region antenna can also be

applied to the case of a stagnation region nose antenna such as that on the second flight. There the plasma occurs at even higher altitudes where vibrational nonequilibrium electron densities are higher than the equilibrium values, and the former condition is expected to apply more so than in the present case. The problem with both results is that for these high altitudes the ratio $\lambda_p/d_E >> 1$ and hence the validity of this plane wave model is uncertain.

The slot antenna model was also applied to the stagnation region.[5] The agreement was again excellent, especially for the vibrational nonequilibrium calculation. Fante[17] examined the power received on the ground in the vicinity of 250 kft where the buildup in plasma was occurring in some detail. The variation with altitude was determined for the basic look angle $\epsilon = 50^{\circ}$. Then at around 250 kft, he constructed the patterns as a function of look angle and found that as the vehicle descended below 253 kft the pattern began to narrow and then below around 249.5, to broaden again. The result is a calculated resonance condition of extremely short duration wherein the attenuation is sharply increased. For the shoulder case the model predicted some resonance phenomena and associated pattern narrowing for 230 kft (vibrational nonequilibrium) or 225 kft (equilibrium). The stagnation effect was not observed in flight. Either its short duration resulted in its occurring between sample times, or else the nonuniformity in the electron density distribution across the antenna surface eliminated that result which was based on a uniform slab model. At the shoulder however the pattern for 225 kft did show considerable nonuniformity as compared to nearby altitudes (see Figures 21 through 24). Whether this can be completely attributed to such a resonance condition, however, is uncertain, since there are so many possible factors affecting the transmission. One related situation which affects the theoretical attenuation distribution has been pointed out. The semi-infinite slabs tend to reduce the transmitted power at angles close to the surface and the ground plane assumption eliminates it in the region $180^{\circ} < \phi_o < 360^{\circ}$.

There are thus a number of questions to be resolved in terms of matching theoretical and actual antenna properties during reentry, but some excellent agreement has been obtained.

5. SUMMARY AND CONCLUSIONS

Flight test S-band antenna data in the shoulder region of the Trailblazer II vehicle have been presented for the third launch on 24 Nov 1970. The antenna results include signal attenuation, reflection, and interantenna coupling. The interpretation of these results involved two types of theoretical analysis. The

17. Fante, R.L. (1972) Private communication.

electrical properties of the high temperature ionized air flowing over the antenna had to be determined. Then various models for predicting antenna behavior in a medium corresponding to those calculations were employed. The analyses produced a complex series of comparisons with various aspects of the flight data, and a number of interesting observations are possible.

(1) The Ball model is a representation of the flow field conditions for low altitudes, especially below 210 kft, whereas the Lew models are more valid above 220 kft. The transition region appears to represent an area where there were some inconsistencies in the predictive trends.

(2) The vibrational nonequilibrium values which freeze the degree of relaxation at the stagnation region levels represent an over-estimation of the electron density, especially at lower altitudes.

(3) Since the vehicle entered at a relatively large angle of attack, the axisymmetric flow results do not strictly apply. For the antenna region the windward orientation should correspond rather closely to the symmetrical results for a slightly stronger shock condition, while the leeward results may be considerably different.

(4) Since the vibrational nonequilibrium results represent increased electron densities at the shoulder, there should be a tendency for these values to be somewhat equivalent to those for the windward angle of attack orientations, especially at the lower altitudes. Both assumptions though should produce higher electron density levels than those of the leeward axis.

(5) The slot antenna reflection results are in good agreement with the data. Below 230 kft, the predictions tend to overestimate slightly. While the rise in plasma effects is matched on the windward side by the vibrational nonequilibrium values, both sets are greater than the leeward data.

(6) The slot antenna results for interantenna coupling are also quite accurate. Above 230 kft the vibrational nonequilibrium is extremely close to the windward data. Both models tend to follow those results rather than the leeward ones, and both predict local maxima although the coupling values at the extremal points differ from the flight values.

(7) The total signal attenuation involves more complex phenomena; it is consequently less clear in its over-all analysis. The slot antenna predictions for the altitude history of the peak value show slightly better agreement for the vibrational equilibrium results, although both models are within about 5 kft of the measured data. There is structure present in both the data and the calculations, and consideration of the entire pattern for $\phi = 59^{\circ}$ indicates that the equilibrium result at 225 kft has the abnormal profile corresponding to the observed pattern at that altitude.

(8) The simplified plane wave results for reflection coefficient have a similar profile to the flight history, although underestimating both windward and leeward data by about 10 kft.

(9) The plane wave attenuation results compared to peak observed values show excellent correspondence for vibrational nonequilibrium and slight underestimation for the equilibrated model. Between 215 kft and loss of signal around 205 kft, the agreement becomes fairly poor. When comparisons with the other antenna models are examined, it becomes clear that these results represent the effect of compensating factors so the agreement is somewhat fortuitous.

(10) Comparison of the three models leads to some additional comments. The three reflection coefficient results agree within 10 kft. The plane wave solution including internal reflections results in a lower attenuation than the slot antenna approach. Thus the effect of pattern on attenuation is a factor which must be given careful consideration.

(11) The results for attenuation at various look angles show that path length has an important effect on attenuation.

(12) Resonances and over-all distribution of power in the antenna pattern depend critically on the interrelation of altitude conditions, look angle, and peak electron density.

The reason for devising the various theoretical models is to acquire representations of the actual flight conditions which are sufficiently accurate to establish a predictive capability for future use. The previous discussions lead to two conclusions in this regard: (1) For antenna properties which depend on peak flow properties close to the surface, such as power reflection coefficient and interantenna coupling, the results of either sophisticated models or simple plane wave methods will be sufficiently accurate; (2) there are, however, other antenna characteristics which depend not only on peak values but on the distribution across the entire shock layer. The wide divergence in total signal attenuation from the various solutions indicates that this type of behavior cannot be treated so generally. The complete slot antenna model is the only one that satisfactorily describes changes in signal gain resulting from the ionization in the flow. This more complete method, coupled to reasonable flow field representations, does allow accurate prediction of the behavior of an antenna system in a reentry environment.

References

1. Poirier, J. L., Rotman, W., Hayes, D. T. and Lennon, J. F. (1969) Effects of the Reentry Plasma Sheath on Microwave Antenna Performance: Trailblazer II Rocket Results of 18 June 1967, AFCRL-69-0354.
2. Hayes, D. T. (1972) Electrostatic probe measurements of flow field characteristics of a blunt body reentry vehicle, AIAA Paper 72-694, 5th Fluid and Plasma Dynamics Conference, Boston, Mass.
3. Hayes, D. T., Herskovitz, S. B., Lennon, J. F., and Poirier, J. L. (1972) Preliminary Report on the Trailblazer II Chemical Alleviation Flight of 28 July 1972, AFCRL-TR-72-0640.
4. Rotman, W., and Maloney, L. R. (1973) High Power Microwave Antenna Performance in the Stagnation Region of a Blunt Reentry Nose Cone, AFCRL-TR-73-0072.
5. Hayes, D. T. and Rotman, W. (1973) Microwave and electrostatic probe measurements on a blunt reentry vehicle, AIAA Journal 11:(No. 5)675-682.
6. Lustig, C. D. and Hayes, D. T. (1969) Observation of electroacoustic resonance in a reentry sheath, Proc. IEEE 57(5):800-802.
7. Karas, N. V. (1972) Microstrip Plasma Probe, AFCRL-TR-72-0417.
8. Aisenberg, S. and Chang, K. W. (1971) Chemical Additives and Diagnostics for High Temperature Air Plasmas, AFCRL-TR-72-0354, Final Rpt, Contract No. AF19(628)-71-C-0077.
9. Lennon, J. F. (1973) Trailblazer II Rocket Tests on the Reentry Plasma Sheath: Vehicle Performance and Plasma Predictions (Flights No. 1-3), AFCRL-TR-73-0317.
10. Fante, R. L. (1967) Effect of thin plasmas on an aperture antenna in an infinite ground plane, Radio Science 2(NS)(No. 1):87-100.

11. Lew, H.G. (1970) Shock Layer Ionization at High Altitudes, AFCRL-70-0702, Final Rpt on Contract F19628-69-C-0112, GE 70SD782, The General Electric Co., Valley Forge, Pennsylvania.

12. Ball, W.H., Webb, H.G., and Lyon, F.J. (1965) Flow Field Predictions and Analysis, Study for Project RAM B3, Space and Information Systems Division Final Rpt No. SID-65-1113, Rpt No. NASA-CR-66106 Contract NAS 1-4743, North American Aviation Inc.

13. Fante, R.L. (1971) Reentry Antenna Test Program, Vol. 2, AVCO System Division Rpt AVSD-0374-69-CR.

14. Poirier, J.L., Antonucci, J.D., and Tropea, D.H. (1973) Performance of a Microwave Antenna System in the Shoulder Region of a Blunt Reentry Nose Cone, AFCRL-TR-73-0656.

15. Russo, A.J. (1963) Estimates of Attenuation and Reflection of Telemetering Signals by Ionized Flow Fields Surrounding Typical Reentry Bodies, NASA Technical Note TN D-1778.

16. Papa, R.J. and Taylor, R.L. (1974) High-Power electromagnetic transmission characteristics of a diffusing reentry plasma, J. Appl. Phys. 45 (No. 2):684-696.

17. Fante, R.L. (1972) Private communication.